Persistent link between Caribbean precipitation and Atlantic Ocean circulation during the Last Glacial revealed by a speleothem record from Puerto Rico

Sophie Warken[1], Rolf Vieten[2], Amos Winter[3], Christoph Spötl[4], Thomas Miller[5], Klaus Peter Jochum[6], Andrea Schröder-Ritzrau[7], Augusto Mangini[1], and Denis Scholz[8]

[1]Heidelberg University
[2]Department of Marine Science, University of Puerto Rico at Mayagüez
[3]Department of Earth and Environmental Systems, Indiana State University
[4]Institute of Geology
[5]Department of Geology
[6]Max Planck Institute for Chemistry
[7]Institute of Environmental Physics, Heidelberg University
[8]Institute for Geosciences

November 24, 2022

Abstract

The high sensitivity of tropical hydro-climate to the mean position of the intertropical convergence zone (ITCZ) at different time scales is well known. However, recent research suggests a more complex behaviour of the northern hemispheric tropical rain belts in the western tropical Atlantic. Here we present a precisely dated speleothem multi-proxy record from a well-monitored cave from Puerto Rico, covering the period between 46.2 and 15.4 ka BP in unprecedented resolution. This allows the investigation of multi-decadal to millennial-scale climate variability. The proxy records document a pronounced response of regional rainfall to abrupt centennial to millennial-scale climatic excursions in the North Atlantic across the Last Glacial (i.e., Heinrich Stadials and Dansgaard/Oeschger events). In particular, we observe a strong agreement between the speleothem proxy data and the strength of the Atlantic meridional overturning circulation, supporting a persistent link of regional precipitation to oceanic forcing. Spectral analysis suggests that multi-decadal to centennial variability persisted in the regional hydro-climate not only during stadial and interstadial conditions, but also during the Last Glacial Maximum, supporting the hypothesis that the Atlantic low-latitude regions respond to internal modes of climate variability on these time scales regardless of the global climate state. The compilation with other paleo-precipitation records enables the reconstruction of past changes in position, strength and extent of the ITCZ in the western tropical Atlantic in response to millennial and orbital global climate change.

Persistent link between Caribbean precipitation and Atlantic Ocean circulation during the Last Glacial revealed by a speleothem record from Puerto Rico

Sophie F. Warken[1,2,3*], Rolf Vieten[4], Amos Winter[4,5], Christoph Spötl[6], Thomas E. Miller[7], Klaus P. Jochum[8], Andrea Schröder-Ritzrau[2], Augusto Mangini[2], and Denis Scholz[1]

[1] Institute for Geosciences, University of Mainz, Germany
[2] Institute of Environmental Physics, University of Heidelberg, Germany
[3] Institute of Earth Sciences, Heidelberg University, Germany
[4] Department of Marine Sciences, University of Puerto Rico, Mayagüez, Puerto Rico
[5] Earth and Environmental Systems Department, Indiana State University, Terre Haute, Indiana, USA
[6] Institute of Geology, University of Innsbruck, Austria
[7] Department of Geology, University of Puerto Rico, Mayagüez, Puerto Rico
[8] Max Planck Institute for Chemistry, Climate Geochemistry Department, Mainz, Germany

Corresponding author: Sophie F. Warken (swarken@iup.uni-heidelberg.de)

Key Points:

- Puerto Rican speleothem record documents multi-decadal to millennial-scale precipitation variability between 46.2 and 15.4 ka BP
- Climate proxies show a distinct rainfall response to abrupt North Atlantic climate change including Heinrich and Dansgaard/Oeschger events
- Compilation of regional precipitation records allows to reconstruct past changes in ITCZ patterns in the western tropical Atlantic

Abstract

The high sensitivity of tropical hydro-climate to the mean position of the intertropical convergence zone (ITCZ) at different time scales is well known. However, recent research suggests a more complex behaviour of the northern hemispheric tropical rain belts in the western tropical Atlantic. Here we present a precisely dated speleothem multi-proxy record from a well-monitored cave from Puerto Rico, covering the period between 46.2 and 15.4 ka BP in unprecedented resolution. This allows the investigation of multi-decadal to millennial-

scale climate variability. The proxy records document a pronounced response of regional rainfall to abrupt centennial to millennial-scale climatic excursions in the North Atlantic across the Last Glacial (i.e., Heinrich Stadials and Dansgaard/Oeschger events). In particular, we observe a strong agreement between the speleothem proxy data and the strength of the Atlantic meridional overturning circulation, supporting a persistent link of regional precipitation to oceanic forcing. Spectral analysis suggests that multi-decadal to centennial variability persisted in the regional hydro-climate not only during stadial and interstadial conditions, but also during the Last Glacial Maximum, supporting the hypothesis that the Atlantic low-latitude regions respond to internal modes of climate variability on these time scales regardless of the global climate state. The compilation with other paleo-precipitation records enables the reconstruction of past changes in position, strength and extent of the ITCZ in the western tropical Atlantic in response to millennial and orbital global climate change.

Plain Language Summary

It is important to understand how rainfall in the western tropical Atlantic might change under a changing climate to ensure the water supply for millions of people. However, it is not well understood, how past rainfall varied in the past thousands of years, especially during the last glacial period, a time of strong climate variability and abrupt climate changes. Here, we use a stalagmite from Puerto Rico to create a new record of past changes in rainfall in this region. For this purpose, we analysed proxy data which reveal a series of wet and dry periods during the Last Glacial corresponding to rapid global climate shifts. Our rainfall-sensitive stalagmite record is able to detect changes in the tropical rainbelt on various timescales, and shows that this variability in rainfall is closely connected to changes in the strength of the ocean circulation. This suggests that the link between the ocean and the atmosphere is more stable than previously assumed. Lastly, comparison of our record with other rainfall-sensitive records from Central America and the northern Caribbean allows a more detailed reconstruction of the spatial and temporal changes of the western tropical Atlantic rainbelt.

1 Introduction

The evolution of precipitation patterns during glacial periods in the tropical Atlantic is a result of competing internal vs. external forcing mechanisms (Lachniet et al., 2009; Schmidt et al., 2004). Our increased understanding of the underlying controls of past precipitation changes provides valuable insight into the climate dynamics involved and more precise boundary conditions for climate models. Last Glacial precipitation reconstructions from the tropical Atlantic have documented pronounced rainfall variability on millennial to centennial timescales including periods of abrupt climate change (Deplazes et al., 2013; Hodell et al., 2008; Peterson et al., 2000). Many of these observations were thought to reflect variable positions of the Intertropical Convergence Zone (ITCZ) in response to changes in cross-equatorial temperature gradients (e.g., Broccoli et al. (2006); Schmidt and Spero (2011); Stríkis et al. (2015)). In particular, prominent millennial-scale alternations, such as Dansgaard/Oeschger (D/O) oscillations and Heinrich events were associated with a pronounced climate response of warm (interstadial) and cold (stadial) periods in the Northern Hemisphere. The generalized assumption is that latitudinal displacements of the ITCZ result from varying strengths of the Atlantic Meridional Overturning Circulation (AMOC) (Henry et al., 2016; Lynch-Stieglitz et al., 2014; McManus et al., 2004). A weaker AMOC coincides with a reduced northward heat transport, a higher cross-equatorial sea-surface temperature (SST) gradient and, consequently, drier conditions in the tropical Northern Hemisphere (Broccoli et al., 2006; Clark et al., 2001; Waelbroeck et al., 2018).

However, the details of the spatio-temporal structure and evolution of the Atlantic ITCZ are still not well understood. For instance, the magnitude and extent of its latitudinal movements, and the role of external forcing, such as insolation, in modulating this variability especially during pronounced and/or abrupt climate change events during glacial periods, such as Heinrich and D/O events, remain unclear. Especially the influence of ocean circulation on changes in Last Glacial tropical rainfall has been subject of recent debates (Burckel et al., 2015; Henry et al., 2016; Roberts & Hopcroft, 2020; Them Il et al., 2015; Waelbroeck et al., 2018). In addition, there is now increasing evidence from both modelling studies as well as proxy records that the simple explanation of a north-south-shifting ITCZ is not adequate to explain the observed rainfall patterns, especially because the most northern shifts of the Atlantic ITCZ are linked to a complex set of forcings and feedbacks on different timescales (Asmerom et al., 2020; Lachniet et al., 2009; Oster et al., 2019; Roberts & Hopcroft, 2020; Singarayer et al., 2017). For instance, a model study by Singarayer et al. (2017) demonstrated that, while asymmetric extratropical forcing (ice sheets, freshwater hosing) generally gives rise to meridional shifts in the zonal

mean tropical rain belt, orbital variations produce an expansion/contraction of the global zonal mean.

Speleothem stable isotope records revealed a pronounced multi-decadal to millennial precipitation dynamic in the western tropical Atlantic (Asmerom et al., 2020; Fensterer et al., 2012; Fensterer et al., 2013; Medina-Elizalde et al., 2010). In a recent study of a 12 ka-long Guatemalan speleothem $\delta^{18}O$ record, Winter et al. (2020) suggested that the evolution of Central American rainfall in the early Holocene was closely related to Caribbean SSTs manifested as a basin-scale response to a more vigorous AMOC. Medina-Elizalde et al. (2017) presented a 3.3 ka-long, sub-decadally resolved speleothem $\delta^{18}O$ record with pronounced multi-decadal variability between 26 and 24 ka BP similar to today, suggesting that the Atlantic low-latitude regions respond to internal modes of climate variability on multi-decadal to centennial scales regardless of the global climate state.

Here we present a stable oxygen isotope record obtained from a speleothem from Larga Cave, Puerto Rico, spanning the time interval from 46.2 to 15.4 ka. Our interpretation of the speleothem oxygen isotopes is supported by trace element (Mg/Ca, Sr/Ca, Ba/Ca) data and $\delta^{13}C$ values, which have been shown to constitute a valuable tool to identify potential hydrological processes or even reconstructing past precipitation patterns (Arienzo et al., 2017; Cruz et al., 2007; Warken et al., 2018). Consequently, our multi-proxy data enables the investigation of changes in the hydrological regime in the western tropical Atlantic during major climate shifts up to sub-decadal resolution.

2 Materials and Methods

2.1 Site description

Larga Cave is located in the north-central karst region of Puerto Rico (18°19'N 66°48'W, Figure 1) at an elevation of about 350 m a.s.l. Since the region of the Greater Antilles is dominated by sea surface, ocean-atmosphere coupling is of great importance for the climate in the Caribbean which nowadays leads to comparatively small temperature variations and can therefore be classified as predominantly maritime (Granger, 1985; Schellekens et al., 2004). In the catchment of the cave, the mean annual air temperature today is 22.5°C, and annual rainfall amount is high with a mean of 2,200mm (Vieten et al., 2018a). According to the observational record from 1980 to 2020 of the closest meteorological station Arecibo observatory (18°21'N 66°45'W, 323m a.s.l, data from http://xmacis.rcc-acis.org/), mean annual air temperature ranges from ca. 20 to 24°C and rainfall amount varies between 600 and 2,700mm. The area

above the cave is covered by dense tropical forest with a thin soil cover that is nearly absent on the higher elevated and exposed locations.

Inside Larga Cave, cave air parameters and various drip sites have been monitored since 2012, showing a constant temperature and relative humidity (rH) regime in the main passage with 22.5 ± 0.2°C and close to 100%, respectively. The cave air pCO_2 variability is dictated by the seasonal cave ventilation with a well-ventilated winter mode (low pCO_2 values) and a near-stagnant summer mode (high pCO_2 values) due to seasonal temperature differences in- and outside the cave (Vieten et al., 2016). The rainfall $\delta^{18}O$ values at the site show a seasonal pattern with more negative (-3 to -5‰ (VSMOW)) values occurring during the wet summer season and higher values (-1 to -2‰ (VSMOW)) in the dry winter season.

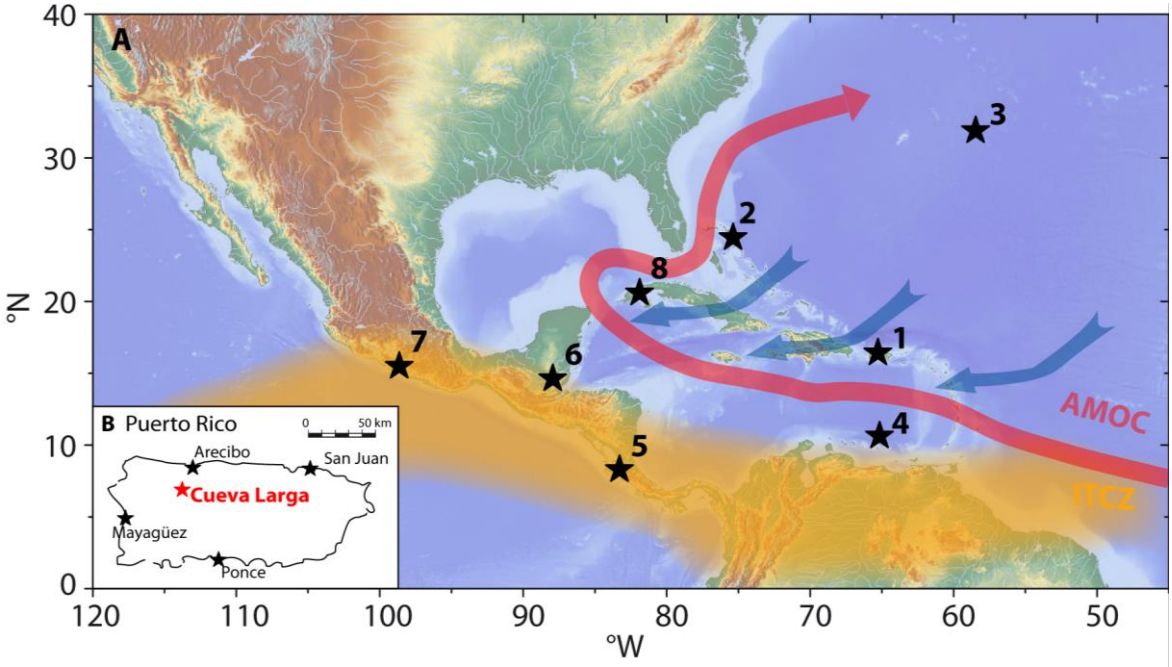

Figure 1 (A) Relevant climatology and sites: (1) Larga Cave (Puerto Rico, this study); (2) Abaco Island (2017; Arienzo et al., 2015); (3) Bermuda Rise (Böhm et al., 2015; Henry et al., 2016; Lippold et al., 2009; McManus et al., 2004); (4) Cariaco Basin (Deplazes et al., 2013; Peterson et al., 2000); (5) Terciopelo Cave (Lachniet et al., 2009); (6) Lake Petén Itzá (Correa-Metrio et al., 2012; Escobar et al., 2012; Hodell et al., 2008); (7) Juxtlahuaca Cave (Lachniet et al., 2013); (8) Santo Tomas Cave (Warken et al., 2019). The yellow shaded area indicates the spatial range of the seasonal migration of the mean position of the ITCZ. The red arrow shows the warm surface current through the Caribbean basin as a part of the AMOC. The blue arrows indicate the mean trajectories of the easterly trade winds and convective systems transporting moisture into the western tropical Atlantic. (B) Location of Larga Cave in north-central Puerto Rico.

The seasonal variations in the $\delta^{18}O$ values of rainwater are smoothed by the soil and karst system acting as a low-pass filter, resulting in a well-mixed seepage water reservoir and a transmission time of atmospheric signals of at least several months to a few years (Vieten et al., 2018a; Vieten et al., 2018b). Therefore, the isotopic composition of drip waters in Larga Cave is relatively constant over the year in most drip sites with a mean of -2.6 ± 0.2‰ (VSMOW) during the monitoring period (2012 – 2019). This value corresponds to the weighted annual mean of the $\delta^{18}O$ valus of -2.5 ± 0.1‰ (VSMOW) (Vieten et al., 2018b). The mean $\delta^{18}O$ value of recently precipitated calcite at different drip sites is -3.1 ± 0.1‰ (VPDB), which indicates that recent calcite precipitation in the cave is near isotopic equilibrium (Hansen et al., 2019; Tremaine et al., 2011). The elemental composition of the drip waters also lacks a clear seasonal cycle with rather stable values for the molar Sr/Ca (0.8 – 1.0 (x 10^{-3})) and Mg/Ca ratios (20 – 30 (x 10^{-3})).

2.2 Stalagmite PR-LA-1

Speleothem PR-LA-1 was collected lying on the cave floor in the main passage (Figure S 1), where the rock overburden is approximately 40 – 80 m. The specimen has a total length of 1.85 m and was removed in five pieces (L1A to L1E, from top to bottom) with individual lengths between 0.25 and 0.55 m (Figure 2). Stalagmite PR-LA-1 consists of whitish and translucent calcite, which in most parts exhibits typical convex-shaped lamination. In the bottom part of subsample L1C, between 110 and 118 cm distance from top (dft), the lamination appears more irregular with a concave "dip" in the middle of the stalagmite (Figure 2). In segment L1E, the part closest to the basis of the stalagmite, several brownish layers indicate detrital inclusions. Slabs were prepared along the growth axis of each segment, which were subsequently used for ^{230}Th/U-dating and stable isotope and trace element analyses.

2.3 Analytical procedures

Samples for ^{230}Th/U-dating were cut along the growth axis using a band saw. Analyses of U and Th isotopes was conducted using a Nu Plasma MC-ICP-MS at the Max Planck Institute for Chemistry (MPIC), Mainz. Chemical preparation of the samples and analytical methods at the MPIC followed Yang et al. (2015) and Obert et al. (2016). All ages and activity ratios were calculated using the half-lives reported by Cheng et al. (2000) in order to preserve comparability with previous publications. Age uncertainties are quoted at the 2σ-level and do not include half-life uncertainties.

Stable isotope samples were drilled with a spatial resolution of 1 mm and analysed at the University of Innsbruck using a ThermoFisher Delta V isotope ratio mass spectrometer equipped with a Gasbench II (Spötl, 2011). Raw data were calibrated against NBS19, and δ-values are reported relative to Vienna Pee Dee Belemnite (VPDB) standard. Long-term precision of the $\delta^{13}C$ and $\delta^{18}O$ values, estimated as the 1σ-standard deviation of replicate analyses, is 0.06 and 0.08‰, respectively (Spötl, 2011; Spötl & Vennemann, 2003).

Element/Calcium ratios of the speleothem were measured by laser ablation ICPMS at the MPIC following the procedure of Jochum et al. (2012) and Yang et al. (2015), using the high-resolution sector-field ICPMS Thermo Element2, combined with the New Wave UP-213 Nd:YAG laser ablation system. The analysed elements were measured at low mass resolution ($m/\Delta m \sim 300$) and are reported to be interference-free (Jochum et al., 2012). Trace element line scans were performed along the growth axis of PR-LA-1 using a spot size of 110 µm and a scan speed of 10 µm/s, resulting in a spatial resolution of 7 µm per data point (scan time 0.7 s). To avoid potential surface contamination, the scan path was pre-ablated with a scan speed of 80 µm/s. In order to account for matrix effects, data reduction was carried out by calculating the blank corrected count rates of the analysed isotopes relative to the simultaneously measured internal standard ^{43}Ca. The reference glass NIST SRM 612 was used for external calibration of the trace element analyses (Jochum et al., 2012; Jochum et al., 2011). Element/Calcium ratios are given in molar units.

2.4 Numerical methods

Correlation analysis was performed with a test statistic based on Pearson's product moment correlation coefficient r (x,y) following a t-distribution with length(x)-2 degrees of freedom. Reported correlation coefficients are all significant at the 0.05 level. Element/Ca ratios were interpolated to the resolution of the stable isotope records for the calculation of the correlation coefficients. The interpretation of the proxy signals is supported by using I-STAL, a model for interpreting Mg/Ca, Sr/Ca and Ba/Ca ratios in speleothems (Stoll et al., 2012), and ISOLUTION 1.0, an isotope evolution model describing the stable oxygen ($\delta^{18}O$) and carbon ($\delta^{13}C$) isotope values of speleothems (Deininger & Scholz, 2019). Spectral analysis was performed using REDFIT (Schulz & Mudelsee, 2002).

3 Results

3.1 Chronology of PR-LA-1

In total, 74 ^{230}Th/U-ages were determined for PR-LA-1 (Figure 2 and Table S **2**), showing that this stalagmite covers the period from 46.2 to 15.4 ka BP with a growth interruption between 41.1 and 35 ka BP. The U content of the samples is about 0.1 - 0.3 µg/g, and in most samples, (^{230}Th/^{232}Th) activity ratios are high, but detrital ^{232}Th content is significant. A number of samples with elevated ^{232}Th are not in stratigraphy with the 'clean' samples, and the inversions persist when using the bulk Earth detrital (^{230}Th/^{232}Th) activity ratio of 0.8 to account for initial ^{230}Th in stalagmite PR-LA-1. Thus, we followed an approach similar to Fensterer et al. (2010) and Beck et al. (2001) to estimate a more appropriate detrital (^{230}Th/^{232}Th) ratio for this stalagmite.

We used linear two-endmember mixing regressions, so called Osmond type I isochrons (Ludwig & Titterington, 1994) for distinct sections with significant ^{232}Th content (Table S **2** and Figure S 2). For each isochron, only subsamples located potentially within a few hundred years (i.e., within a distance of 1-5cm, depending on the growth rate) were selected to meet the assumption of nearly coeval deposition.

The slope of each linear correction model (Figure S 2) yielded an estimate for a more appropriate detrital (^{230}Th/^{232}Th) ratio (Wenz et al., 2016). With this approach, we derived isochron slopes between 7.04 and 22.22 for seven sections (Table S **1**), with an overall mean of 16.46 ± 10.58. Three isochrons show a correlation coefficient of $r < 0.9$, which could be related to the relatively low variability in (^{232}Th/^{238}U), but it may also indicate that the assumption of coeval deposition was not applicable. Taking into account only the correction models with $r > 0.9$, yields a mean correction factor of 19.79 ± 4.93, which was subsequently used to correct the measured U and Th activity ratios and to calculate the ages. The obtained correction factor suggests a very high ^{230}Th contribution from cave seepage water or non-carbonate contamination compared to the commonly used bulk Earth ratio of 0.8 (Wedepohl, 1995). The composition of the initial or detrital phase can be very different from this value, e.g., due to partial leaching effects, Th adsorption, alpha recoil or non-silicate origin of the detrital phase prior to deposition (Hellstrom, 2006). Consequently, (^{230}Th/^{232}Th) activity ratios of up to 18.7 for tropical limestones have been reported by a number of studies from the Bahamas, Cuba and Puerto Rico, supporting our result (Arienzo et al., 2015; Beck et al., 2001; Fensterer et al., 2010; Rivera-Collazo et al., 2015). However, in contrast to other studies, which assumed uncertainties of the correction as high as 100%, our isochron approach yields a relatively low error for the

Th activity ratio of about ±25 %. Hence, even though the correction itself is relatively large, the propagated uncertainty due to the correction is small for nearly all corrected ages. Even for samples with the lowest ($^{230}Th/^{232}Th$) activity ratio age uncertainties remain below 5%.

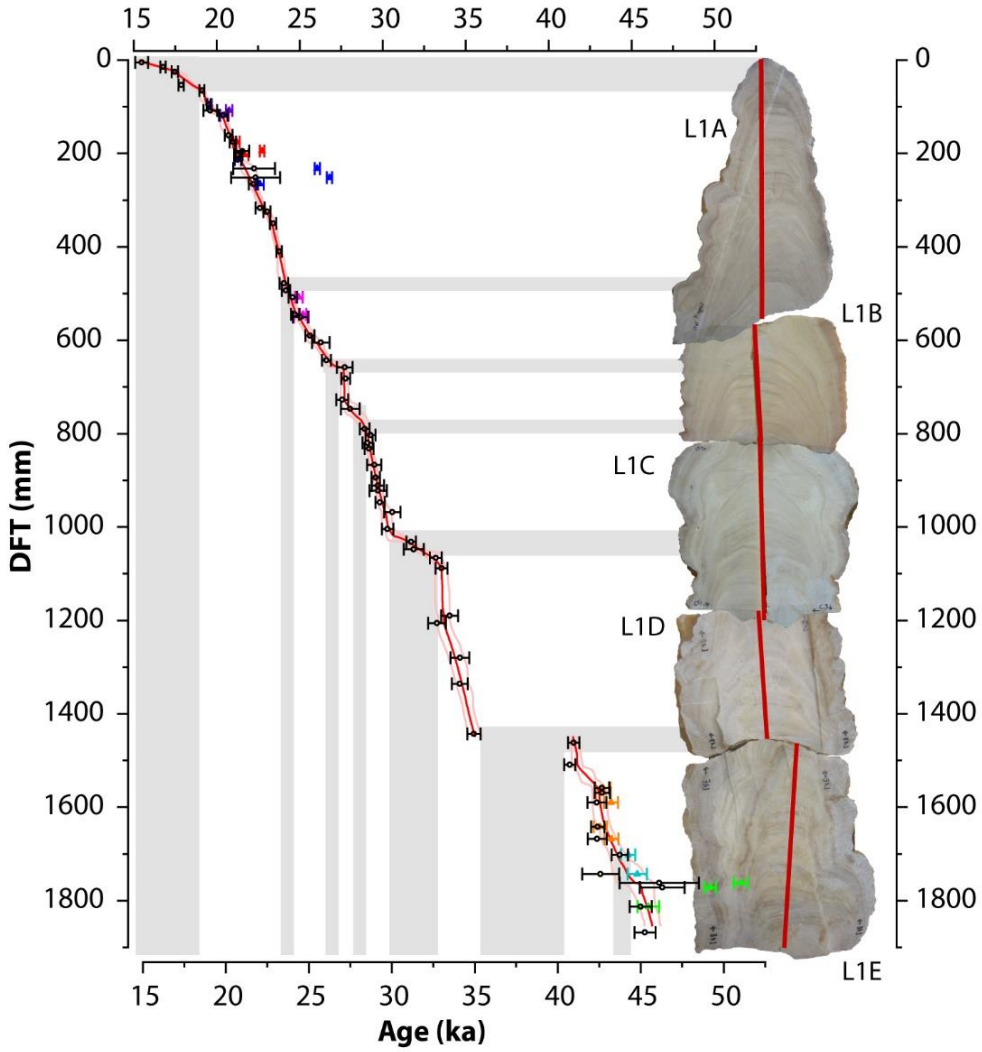

Figure 2: Corrected $^{230}Th/U$ data (black) and age model (red) calculated using StalAge (Scholz & Hoffmann, 2011). The uncorrected ages used for the isochrons in Figure S 2 are shown in corresponding colors. Grey bars indicate periods of reduced or absent speleothem deposition. Right side: scan of the individual segments (L1A to L1E) of speleothem PR-LA-1, with approximate position of the growth axis shown by the red straight lines.

After this correction, 9 of 74 samples of PR-LA-1 are still not in chronological order (Figure 2). These reversals might be due to diagenetic alteration, indicated by partly lower U concentrations, or changes in the initial ^{230}Th contribution from the detritus or seepage water. For these reasons, and considering the good agreement of the surrounding ages within the tight chronology, we did not include these ages in the final age model. The applied methods allow to construct an overall precise chronology with average uncertainties of 0.5 to 1.5 % of the corrected ages using the algorithm StalAge (Scholz & Hoffmann, 2011). This corresponds to errors in the chronology in the order of 200 to 400 years before 30 ka BP and 90 to 200 years afterwards. In sections with lower sampling density and/or significant detrital Th, the uncertainty increases up to 500 – 1000 years, which applies mostly to the bottommost sections, such as in segments L1E (45.5 and 44 ka BP) and L1C (35.5 to 33.5 ka BP).

The average growth rate is in the order of 100 µm/a, but the age model suggests very fast rates of up to more than 1 mm/a between 43.2 – 43.0, 41.5 – 41.1, 33.7 – 33.5 and 27.8- 27.6 ka BP. Comparably low deposition rates down to 10 – 30 µm/a occurred between 43.2 – 41.3, 33.5 – 30.3, 28.9 – 27.8 and 17.5 – 15.4 ka BP, as indicated by the grey bars in **Figure** 2.

3.2 Speleothem climate proxy patterns

Figure 3 shows the speleothem $\delta^{18}O$ and $\delta^{13}C$ values as well as the Mg/Ca, Sr/Ca and Ba/Ca records. In the earlier part of the record, from 46.2 to about 17 ka, the three element ratios show a variability of roughly ±50% around the mean values, with a Mg/Ca baseline of 1.0 ± 0.5mmol/mol, and Sr/Ca (Ba/Ca) values of 0.06 ± 0.03 mmol/mol (0.08 ± 0.04 µmol/mol). After 17 ka, Mg/Ca, Sr/Ca and Ba/Ca values strongly increase towards their highest values of the whole record. $\delta^{18}O$ and $\delta^{13}C$ values show a similar pattern with $\delta^{18}O$ values around 0 ± 2‰, and reaching the highest values of 1 - 2‰ between 17 and 15.4 ka, whereas $\delta^{13}C$ values vary around -9 ± 3‰. On longer timescales, $\delta^{13}C$, $\delta^{18}O$, and Mg/Ca values follow the general pattern of the speleothem growth rate (Figure 3). Regarding the whole record between 15.4 and 46.2 ka, $\delta^{18}O$ and $\delta^{13}C$ values show a strong correlation ($r_{\delta 13C/\delta 18O} = 0.52$) and a similar pattern with Mg/Ca values ($r_{Mg/\delta 18O} = r_{Mg/\delta 13C} = 0.40$). Sr/Ca and Ba/Ca are also correlated ($r_{Sr/Ba} = 0.49$), but show only a weak relationship with Mg/Ca ($r_{Mg/Sr} = 0.32$).

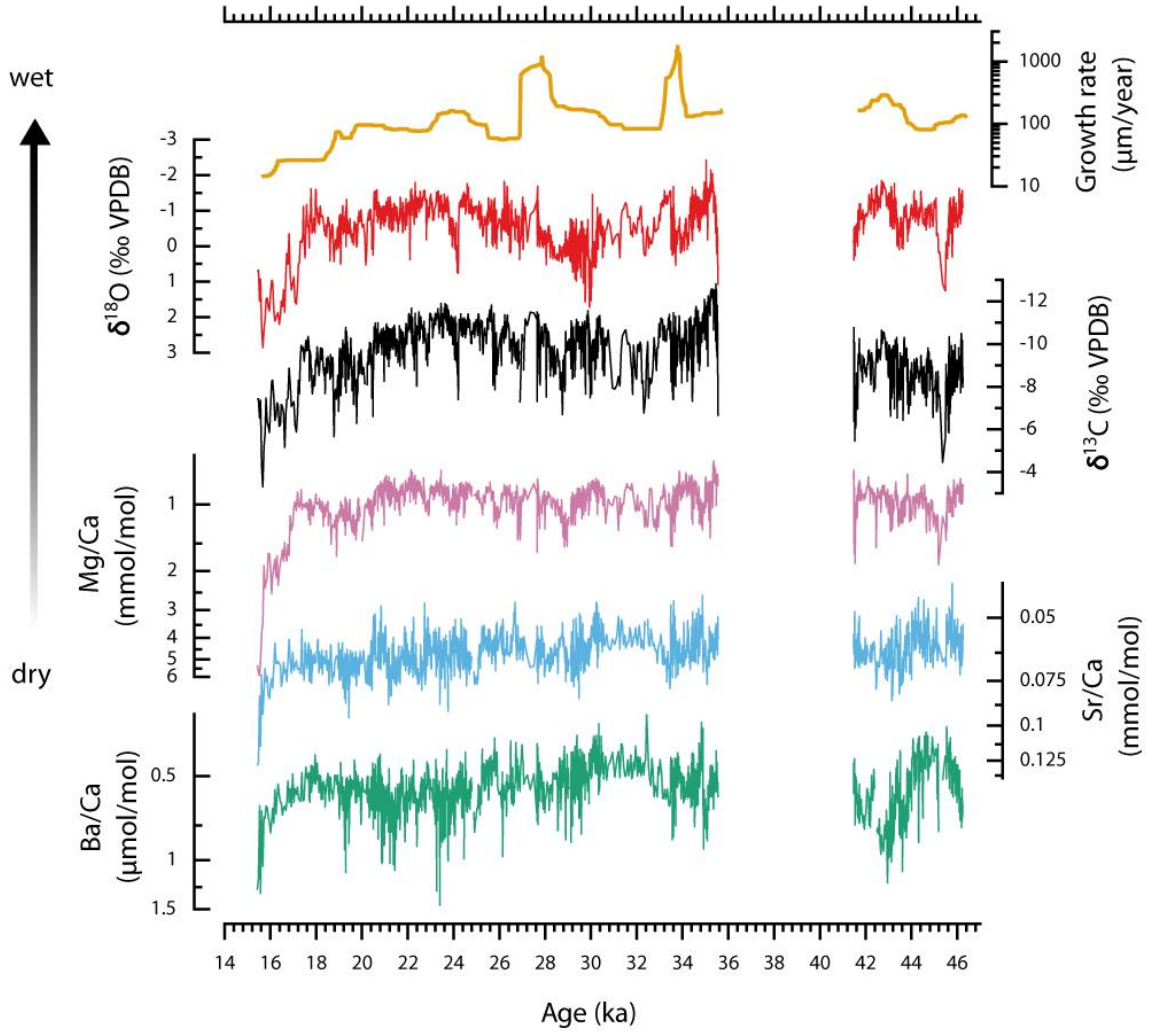

Figure 3: Speleothem climate proxies in PR-LA-1 (from top to bottom): Growth rate (dark yellow, derived from the age model); stable isotopes of oxygen ($\delta^{18}O$ values, red), stable isotopes of carbon ($\delta^{13}C$ values, black); Mg/Ca (purple); Sr/Ca (blue); and Ba/Ca (green). Note the inverted scale of all proxies, which indicates the interpretation as proxies for wet/dry conditions (section 4). Mg/Ca, Sr/Ca and Ba/Ca are plotted on a logarithmic scale.

3.3 Spectral analysis

For periods of relatively slow growth (with deposition rates in the order of 10 µm/a), the temporal resolution of the stable isotopes is on centennial timescales. For intervals with higher growth rates of up to 1 mm/a, even multi-decadal scales are resolved. To assess the power of sub-millennial variability of the proxies, spectral analysis was performed using REDFIT (Schulz & Mudelsee, 2002) for different time slices across the record. For this purpose, stadial and interstadial periods were chosen with a) relatively high growth rate to allow for multi-decadal resolution, and b) at least 500 years of continuous coverage. This includes the Last Glacial Maximum (LGM, 24 – 18 ka BP), Greenland stadials 3 (27 - 24.3 ka BP), 5.1 (30.2 - 28.7) and 7 (34.3 – 33.7 ka BP), Greenland interstadials 7 (35.4 – 34.3 ka BP), 11 (43.3 – 41.5 ka BP) and 12 (45.0 – 43.9 ka BP) as well as Heinrich stadials 1 (17.5 – 15.4 ka BP) and 2 (24.2 – 23.8 ka BP). The $\delta^{18}O$ spectra show enhanced power in multi-decadal to centennial periods during the LGM, Greenland stadials and interstadials (Figure 4). The spectral power variability of $\delta^{13}C$ and Mg/Ca is generally weaker, but they also show enhanced power for multi-decadal periods (**Figure S 5** and **Figure S 6**).

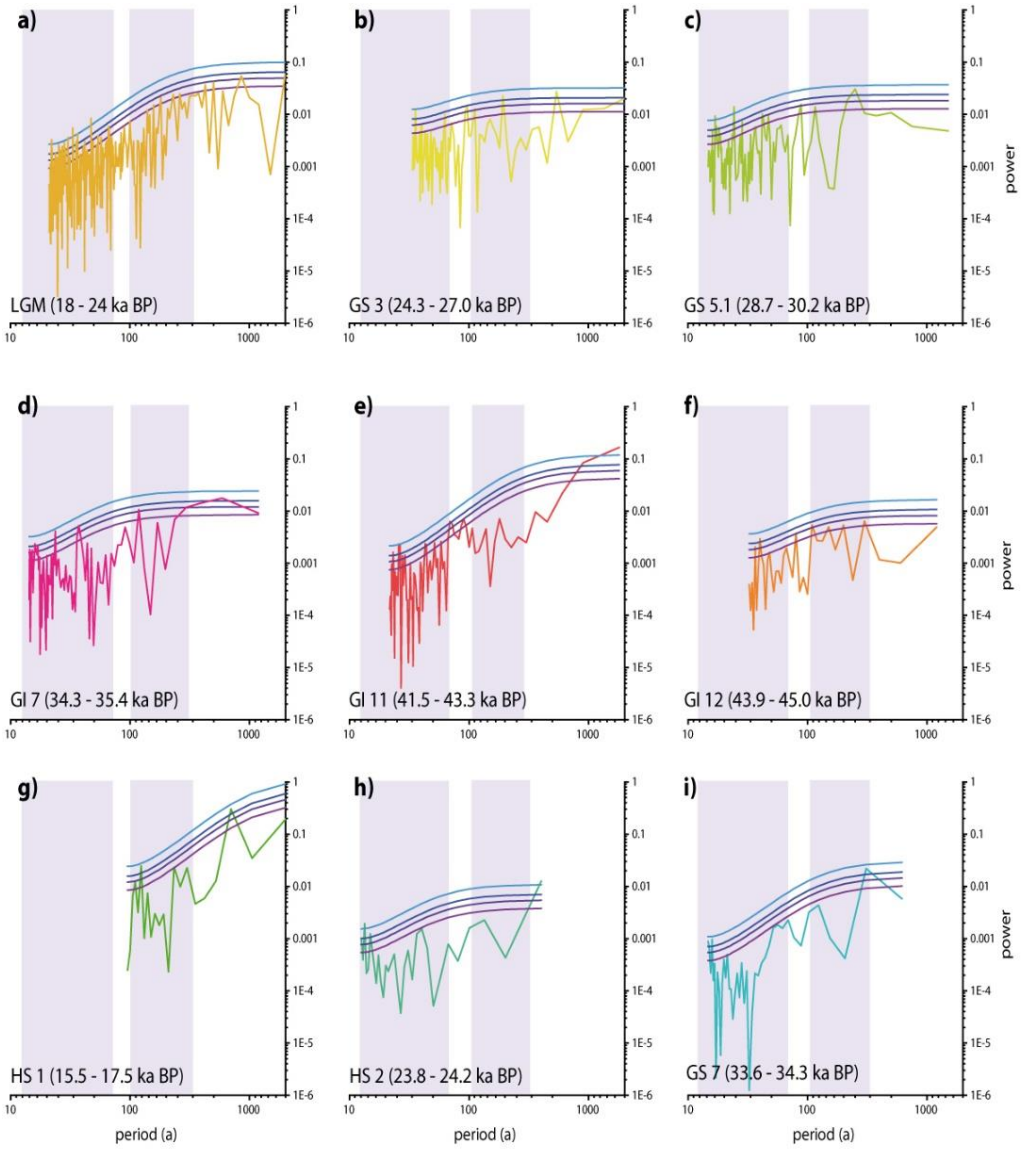

Figure 4: Spectral power for different intervals of the PR-LA-1 $\delta^{18}O$ record calculated with REDFIT (Schulz & Mudelsee, 2002). Coloured lines indicate the calculated AR(1) false-alarm levels of 80% (purple), 90% (violet), 95% (dark blue) and 99% (light blue), respectively. Purple rectangles indicate the multi-decadal and centennial period bands. For all shown spectra, the AR(1) passed the REDFIT runs test, which checks the equality of theoretical AR(1) and data spectrum.

4 Discussion

4.1 Climate proxy variability and interpretation

4.1.1 Inferences from modelling of cave and karst processes

Speleothem PR-LA-1 grew during the second half of the last glacial period (115 – 11.7 ka BP), when the climate in the Caribbean area was generally drier compared to the Holocene (Correa-Metrio et al., 2012; Hodell et al., 2008; Peterson et al., 2000; Schmidt & Spero, 2011), and Caribbean SST reconstructions (Hagen & Keigwin, 2002; Lea et al., 2003) report colder temperatures by 2 - 4°C. The PR-LA-1 $\delta^{18}O$ record exhibits a pattern of millennial-scale variability reminiscent of Dansgaard/Oeschger oscillations recorded in Greenland ice cores (Figure 5), which is also visible in other proxies, such as $\delta^{13}C$ and Mg/Ca (Figure 3), indicating a common driving process. In agreement with previous hydro-climate reconstructions from the tropical Atlantic realm (Arienzo et al., 2017; Lachniet et al., 2009; Winter et al., 2020), we associate lower (higher) speleothem $\delta^{18}O$ values during interstadial (stadial) phases with wetter and warmer (drier and cooler) conditions and greater (less) convective rainfall intensity.

In the main passage of Larga Cave, where PR-LA-1 was collected, Vieten et al. (2016) found a pronounced present-day seasonal cave air pCO_2 cycle, with a well-ventilated (i.e., low pCO_2) regime during the dry winter season and a near-stagnant, high pCO_2 mode during the wet summer. In addition, drip interval variations on intra- and inter-annual scale in response to recharge have been observed in Larga Cave at modern drip sites (Vieten et al., 2018b;Vieten et al., 2018a). In combination with the observed co-variation of speleothem stable isotope and trace element ratios (Figure 3), we suggest a strong hydrological control of these proxies influenced by cave and karst processes and the saturation state of the drip water (Cruz et al., 2007; Sinclair et al., 2012; Wassenburg et al., 2019). The degree of supersaturation is determined by cave air temperature and pCO_2, the initial Ca concentration and the degree of prior calcite precipitation (PCP). Longer drip intervals may further coincide with an increase in PCP and result in higher Mg/Ca, Sr/Ca and Ba/Ca ratios (Mattey et al., 2010; Stoll et al., 2012) as well as higher $\delta^{18}O$ and $\delta^{13}C$ values (Dreybrodt & Scholz, 2011; Hansen et al., 2019) of the drip water. A higher degree of PCP also decreases the saturation state of the drip water and therefore slows down stalagmite growth, reducing the partitioning of Sr and Ba, which may explain weak or even absent correlations of these elements in stalagmite PR-LA-1 (Stoll et al., 2012; Warken et al., 2018). Enhanced cave ventilation also leads to lower pCO_2 in the cave atmosphere and accordingly lower Ca equilibrium concentrations (Baker et al., 2014; Mattey

et al., 2010). We regard these processes as very likely to act as controlling elements of drip water saturation and varying elemental and isotopic signatures in speleothems from Larga Cave. Numerical simulation of the observed elemental variability in stalagmite PR-LA-1 with I-STAL (Stoll et al. (2012), supplementary material S1) support this interpretation. For instance, the simulations indicate that the drip of PR-LA-1 indeed experienced a large drip interval variability (Figure S 3) and a variable effective cave air pCO_2 (i.e., the pCO_2 recorded by the stalagmite during the season of main calcite precipitation), which is potentially linked to seasonally variable ventilation. The influence of these processes on the $\delta^{18}O$ and $\delta^{13}C$ values of the speleothem was additionally explored using the ISOLUTION model (Deininger and Scholz (2019), supplementary material S1). This analysis reveals that the highest speleothem $\delta^{18}O$ (and $\delta^{13}C$) values can only be explained by assuming drip water values of 0 ‰ for $\delta^{18}O$ (-6‰ for $\delta^{13}C$), which is significantly higher than the modern values of -2.6 ‰ (and -13‰). This suggests that the observed magnitude of the excursions in the stable isotope record cannot be explained solely by cave-internal isotope fractionation effects during calcite precipitation, but must partially originate from the composition of the infiltrating water, which is, in turn, related to changes in the environmental conditions above the cave.

4.1.2 Speleothem $\delta^{18}O$ values as a proxy for regional precipitation amount and convective intensity

In Larga Cave, drip water $\delta^{18}O$ values predominantly represent rainfall $\delta^{18}O$ values, which are linked to rainfall amount (Vieten et al., 2018a; Vieten et al., 2018b). Therefore, we consider speleothem $\delta^{18}O$ values as a proxy of past precipitation and convective activity in the western tropical Atlantic, which enables us to reconstruct changes of last Glacial precipitation patterns. Compared to modern calcite (-3.1‰), $\delta^{18}O$ values in speleothem PR-LA-1 are about 3-4‰ higher with an average level of about 0±1‰ during the LGM, which cannot solely be explained by cave and karst processes (section 4.1.1). On glacial-interglacial timescales, a number of additional effects can significantly impact the $\delta^{18}O$ values of drip water and speleothems, such as the changing $\delta^{18}O$ value of source waters due to increased continental ice volume, lower SSTs and salinity values (Baker & Fritz, 2015). For the (sub)tropical Atlantic, these account for a change in the $\delta^{18}O$ value of sea water of up to 2‰ during glacial periods (Hagen & Keigwin, 2002; Schmidt & Spero, 2011), which reduces the effective difference between modern calcite and speleothem PR-LA-1 $\delta^{18}O$ values to about 2‰. This suggests that Puerto Rico experienced a drier and predominantly non-convective regime during glacial times.

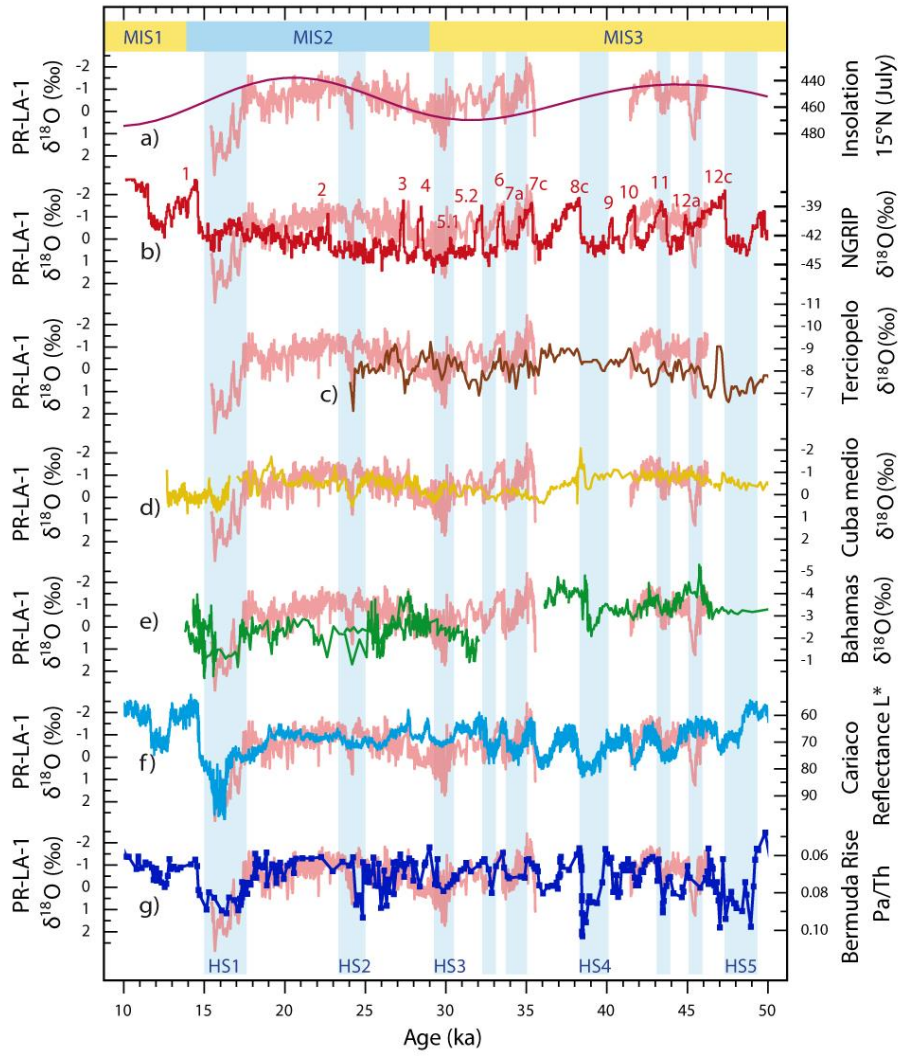

Figure 5: PR-LA-1 $\delta^{18}O$ values in comparison with (from top to bottom) (a) 15°N summer insolation (axis inverted); (b) $\delta^{18}O$ values from the NGRIP ice core using the GICC05 timescale (Svensson et al., 2008). Numbers indicate the Greenland interstadials after Rasmussen et al. (2014); (c) speleothem $\delta^{18}O$ values from Terciopelo Cave, Costa Rica (Lachniet et al., 2009); (d) speleothem $\delta^{18}O$ values from Santo Tomas Cave, Cuba (Warken et al., 2019); (e) $\delta^{18}O$ values from Abaco island, Bahamas (Arienzo et al., 2017); (f) Reflectance record from the Cariaco basin off Venezuela reflecting the mean meridional position of the ITCZ (Deplazes et al., 2013); (g) $^{231}Pa/^{230}Th$ compilation from the Bermuda Rise reflecting the strength of the AMOC (Böhm et al., 2015; Henry et al., 2016; Lippold et al., 2009; Lippold et al., 2019; McManus et al., 2004). Vertical blue bars indicate intervals of weak AMOC, such as Heinrich stadials 1-5.

Compared to the modern average annual rainfall amount at Larga Cave, an increase of 1‰ in $\delta^{18}O$ values roughly corresponds to a rainfall decrease of about 50% (Vieten et al., 2018a). However, we regard this value as an upper limit. Enhanced moisture recycling has been observed at the location of Larga Cave during the dry season and is especially visible in the d-excess of rainwater (Vieten et al., 2018b). This mechanism may shift the weighted annual mean of the $\delta^{18}O$ values of the drip water towards higher values. Thus, the relative change of precipitation amount could be overestimated. The difficulty of quantifying this effect for the last glacial period prohibits a robust calibration of glacial speleothem $\delta^{18}O$ values with rainfall. Enhanced moisture recycling may be of particular importance for the driest intervals of our record, of which Heinrich Stadial 1 (17 to 15.4 ka BP) stands out, where speleothem $\delta^{18}O$ values (and all other proxies) show a strong increase of up to 6‰ compared to modern calcite. A decreased temperature of about 4°C during the coldest intervals of the Last Glacial compared to recent times (Arienzo et al., 2015) would only explain about 1‰ change in cave temperature-related isotope fractionation during carbonate precipitation. As discussed in section 4.1.1 and the supporting information S1, disequilibrium isotope fractionation effects during very cold and dry intervals would lead to a maximum change of +1-2‰, thus still leaving a residual shift in speleothem $\delta^{18}O$ values of about 1-2‰, which cannot be explained by glacial boundary conditions (Arienzo et al., 2017; Escobar et al., 2012). We note that a calibration study from the north-eastern Yucatán peninsula (Medina-Elizalde et al., 2017) suggested that local precipitation varied between +200% and −100% between 26 and 23 ka BP (including Heinrich stadial 2), while speleothem $\delta^{18}O$ values ranged from -6 to 0‰, which translates in a similar slope as observed in this study. This confirms that our inferences are reasonable.

In contrast, the most negative $\delta^{18}O$ values in PR-LA-1 of approximately -1.9 to -2.4‰ were reached during Greenland Interstadials (GI) 7c (35.4 - 35.0 ka) and 11 (43.3 – 42.2 ka). Similarly, GIs 2, 3, 5, 6, 12a and 12c are characterized by $\delta^{18}O$ values of about -1.2 to -1.6‰, whereas during GI 4 and 4.1, the values stay around -1‰ (Figure 5). Taking into account only the global ice volume and salinity changes in the tropical Atlantic surface waters during Marine Isotope Stage (MIS) 3, which account for about 0.5-1‰ (Hagen & Keigwin, 2002; Schmidt & Spero, 2011), peak values during GI7c and 11 nearly reach modern values in the cave. Keeping in mind that speleothem records from Puerto Rico and other Caribbean sites exhibit $\delta^{18}O$ variations of up to ± 1‰ during the Holocene (e.g., Fensterer et al. (2013); Medina-Elizalde et al. (2010); Winter et al. (2011)), we conjecture that the environmental conditions could have been comparable to the present-day. During the other interstadials, $\delta^{18}O$ values suggest at most only slightly drier and/or cooler conditions.

4.1.3 Persistent link of multi-decadal to millennial-scale rainfall to ocean circulation

A remarkable feature of the PR-LA-1 record is that speleothem $\delta^{18}O$ values closely track changes in the reconstructed strength of the AMOC (Figure 5) on centennial to millennial scales. Major events of freshwater input into the North Atlantic and subsequent slowdown of ocean circulation, such as Heinrich stadials HS1 (17.2 - 15.5 ka), HS2 (24.3 - 23.8 ka) and HS3 (30 – 29 ka), are recorded by elevated speleothem $\delta^{18}O$ values (Figure 5 and Figure 6), indicating pronounced transitions to drier and cooler conditions on Puerto Rico (section 4.1.2). Similar observations were made in other studies. A cooling by about 4°C during HS 1 to 3 was observed in speleothems from the Bahamas (Arienzo et al., 2017; 2015). Lacustrine sediments from Central America show increased aridity and a 4-10°C cooling associated with HS1 (Correa-Metrio et al., 2012; Escobar et al., 2012; Hodell et al., 2008), and a speleothem record from south-western Mexico demonstrates a reduction of the North American Monsoon (Lachniet et al., 2013).

The Larga $\delta^{18}O$ record strikingly agrees with sedimentary $^{231}Pa/Th$ from the Bermuda Rise, not only during Heinrich stadials, but also in the course of millennial to centennial variations associated with D/O main- and sub-stages (Figure 5). This suggests a strong and persistent link between Puerto Rican precipitation and the AMOC, which we therefore regard as the dominant regional control of abrupt rainfall changes in the subtropical Caribbean (Burckel et al., 2015; Henry et al., 2016; Waelbroeck et al., 2018). In agreement with recent modelling studies suggesting that asymmetric extratropical forcing, such as ice sheets or freshwater input into the North Atlantic, produce meridional shifts in the zonal mean rain belt, these observations indicate a southward shift of the ITCZ associated with abrupt decreases of AMOC strength (Broccoli et al., 2006; Clark et al., 2001; Singarayer et al., 2017).

Variations in the strength of the AMOC are linked to meridional redistribution of ocean heat within the North Atlantic, whose spatial SST pattern is superimposed on that of the Atlantic Multi-Decadal Oscillation (AMO) (Winter et al., 2020; Zanchettin et al., 2014; Zhang & Zhang, 2015). In particular, this Atlantic multi-decadal variability also involves surface warming and cooling of the inter-American Seas (del Monte-Luna et al., 2015; Enfield et al., 2001). Spectral analysis of the speleothem PR-LA-1 $\delta^{18}O$ data indicates relatively high power on multi-decadal to centennial periods during Greenland Stadials and Interstadials as well as the LGM. Instrumental, paleoclimate and modelling data support a positive correlation between the AMO and the hydro-climate over the western tropical Atlantic including Puerto Rico during the Late Holocene as well as on millennial and longer time scales (e.g., Bhattacharya et al. (2017); Fensterer et al. (2012); Winter et al. (2011)).

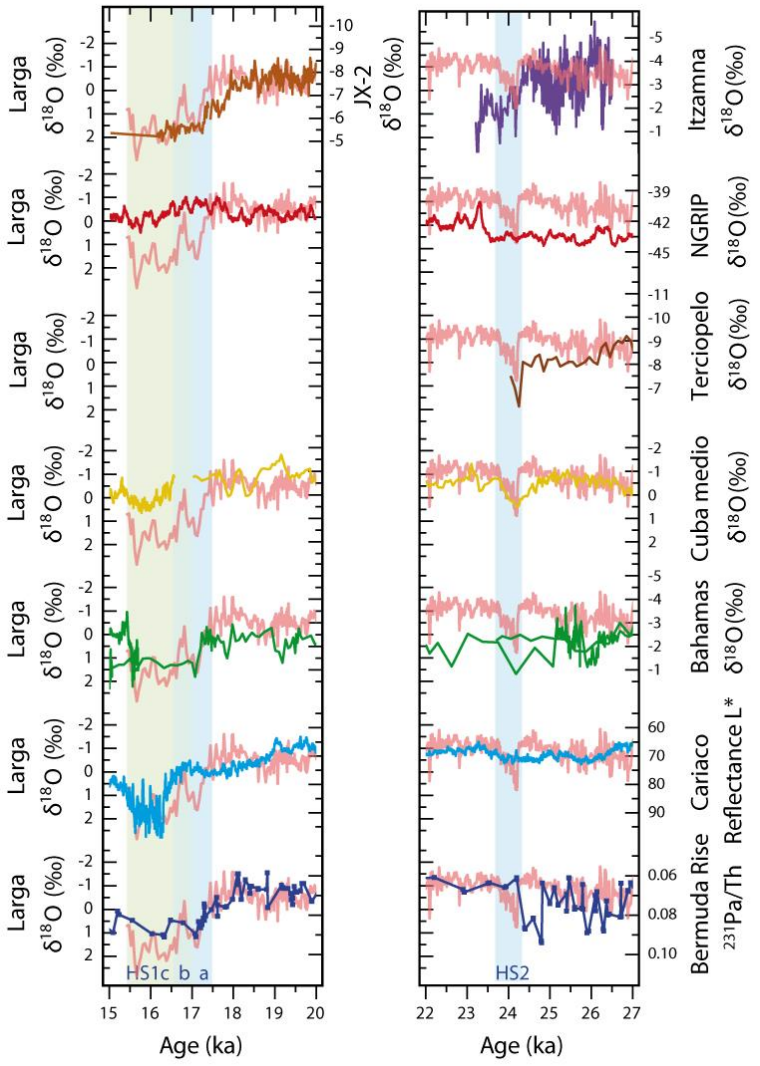

Figure 6: PR-LA-1 $\delta^{18}O$ record for Heinrich stadials 1 (left) and 2 (right) in comparison with: $\delta^{18}O$ values from the NGRIP ice core using the GICC05 timescale (Svensson et al., 2008).; speleothem Cuba Medio $\delta^{18}O$ values from Santo Tomas Cave, Cuba (Warken et al., 2019); $\delta^{18}O$ values from Abaco Island, Bahamas (Arienzo et al., 2017); reflectance record from the Cariaco Basin (Deplazes et al., 2013) and $^{231}Pa/^{230}Th$ compilation from the Bermuda Rise (Böhm et al., 2015; Henry et al., 2016; Lippold et al., 2009; McManus et al., 2004). Also shown in the top left panel are speleothem $\delta^{18}O$ values from Juxtlahuaca, Mexico (Lachniet et al., 2013). On the top right panel, $\delta^{18}O$ values from Río Sécreto, Yucatán Peninsula, Mexico (Medina-Elizalde et al., 2017) and speleothem $\delta^{18}O$ values from Terciopelo cave, Costa Rica (Lachniet et al., 2009) are presented. Vertical blue and green bars indicate the (sub-) stages HS1 (left) and HS2 (right) as registeredd in the PR-LA-1 $\delta^{18}O$ record.

For the Last Glacial, the lacustrine record from Lake Petén Itzá also suggests inter-annual and multi-decadal variability (Correa-Metrio et al., 2012; Escobar et al., 2012; Hodell et al., 2008), and Medina-Elizalde et al. (2017) reported multi-decadal variability in a high-resolution speleothem $\delta^{18}O$ record from the Yucatan Peninsula spanning 26 to 24 ka BP (Figure 6). Our dataset indicates that multi-decadal variability is indeed a persistent feature of the tropical hydro-climate during both interstadials and stadials as well as across the LGM. This supports the hypothesis that the Atlantic low-latitude regions responded to internal modes of climate variability on these timescales regardless of the global climate state (Medina-Elizalde et al., 2017; Winter et al., 2020). The appearance of multi-decadal, centennial and millennial scale precipitation variability in the same archive further suggests a common mechanism of heat redistribution in an AMO-analogue mode on all these timescales (Bhattacharya et al., 2017; Ting et al., 2009; Zhang & Zhang, 2015). This argues for a dominant role of the strength of ocean circulation in tropical Atlantic precipitation and adds support to the hypothesis that the AMOC is a key element for the link between northern high latitudes and tropical climate - not only during Heinrich stadials but also for D/O events.

4.2 Spatio-temporal patterns of western tropical Atlantic precipitation

4.2.1 Spatio-temporal patterns on orbital timescales

The compilation of existing reconstructions of past precipitation in the western tropical Atlantic realm provides the opportunity to explore spatio-temporal rainfall patterns and to reconstruct past regional ITCZ variations on millennial to orbital timescales. Figure 5 shows that the long-term variability in PR-LA-1 $\delta^{18}O$ values generally appears to be inversely related with summer insolation. This observation agrees with long speleothem records from Cuba and Costa Rica, which also document an inverse relationship of regional rainfall and summer insolation during MIS 4 to 2 (Lachniet et al., 2009; Warken et al., 2019). This relationship is unexpected since previous studies have documented a positive link between rainfall intensity and summer insolation in the Americas (Cruz et al., 2009; Poveda et al., 2006). However, model studies also demonstrated that the seasonal northern limit of the American rain belt during the Last Glacial varied not only in response to local insolation, but also responded to ice-sheet forcing due to the regional land-ocean configuration (Singarayer et al., 2017). During times of an extensive Northern Hemisphere ice cover, the maximum northward extent of the ITCZ occurs earlier in the year, when most local land is to the south (Singarayer et al., 2017). When local summer insolation is high, the land-sea temperature contrast increases and the ITCZ rain belt moves south, apparently away from the warmer hemisphere, but in fact towards the locally warmed

land (Singarayer et al., 2017). This implies that orbital variations produce expansions and contractions of the global zonal mean of the ITCZ. We further evaluate this process here by comparing the speleothem records from the northern limit of the tropical rain belt to the reflectance record from the Cariaco basin, which mirrors the meridional position of the mean position of the ITCZ (Deplazes et al., 2013). During periods of reduced summer insolation, e.g., MIS2, $\delta^{18}O$ values of speleothems north of the Cariaco basin as well as central American lacustrine sediments (e.g., Hodell et al. (2008)) indicate relatively wet conditions. In contrast, the Cariaco reflectance record remains relatively constant, which may suggest that the tropical rain belt indeed expanded northward during this interval in response to orbital forcing.

4.2.2 Spatio-temporal patterns on millennial timescales

Of all the Heinrich stadials recorded in PR-LA-1, HS1 (17.2 - 15.4 ka) stands out as the most pronounced, suggesting that it was the severest stadial in the region (Arienzo et al., 2015; Escobar et al., 2012). This observation is supported by reconstructions of AMOC strength showing that HS1 was accompanied by a near shutdown of the AMOC and an abrupt and synchronous response of the ITCZ to changes in ocean circulation (Lachniet et al., 2013; Stríkis et al., 2015). In contrast, there were only muted changes during HS2 and 3 (Böhm et al., 2015; Lynch-Stieglitz et al., 2014). The onset of HS1 in PR-LA-1 occurred at about 17.5 ka with a gradual increase in $\delta^{18}O$ values indicating a decrease of rainfall amount and temperature, interrupted by a short warm and wet period at about ~17 ka (Figure 6). Comparing PR-LA-1 $\delta^{18}O$ values with the speleothem record from Juxtlahuaca Cave, Mexico (Lachniet et al., 2013), and Abaco Island, Bahamas (Arienzo et al., 2017), shows that the timing of the increase in the $\delta^{18}O$ values during the sub-stages of HS1 was nearly synchronous (Figure 6). A three-stage structure of HS1 is also recorded by lacustrine sediments in Guatemala (Escobar et al., 2012), supporting its region-wide impact.

In contrast, HS2 on the other hand shows a slightly different picture in Puerto Rico characterized by an abrupt, one-stage increase in $\delta^{18}O$ between 24.2 and 23.8 ka (Figure 6), which is also clearly imprinted in the records from the Bahamas and Cuba. The records from the north-eastern Caribbean closely follow the pattern of $^{231}Pa/Th$ on the Bermuda Rise, indicating a temporary weakening of the AMOC and a synchronous reduction of regional rainfall. In contrast, the speleothem record from the Yucatan peninsula (Medina-Elizalde et al., 2017) is characterized by a continuous precipitation reduction after 23.8 ka (Figure 6), which was attributed to be synchronous and in-phase with precipitation records from South America. The difference in the climate response in the north-eastern Caribbean compared to

519 reconstructions from further south-west most likely indicates a diminishing influence of the
520 Atlantic from the east towards the south-west.
521 In addition, the amplitude of stadial and interstadial intervals is attenuated in the northernmost
522 records from Cuba and the Bahamas (Arienzo et al., 2017; Warken et al., 2019), but also
523 towards Costa Rica (Lachniet et al., 2009) compared to precipitation records in the Cariaco
524 basin (Deplazes et al., 2013) and in Larga Cave (Figure 5). Warken et al. (2019) noted a weaker
525 sensitivity of $\delta^{18}O$ values in a speleothem from Cuba to North Atlantic forcing during MIS 4 to
526 2 compared to MIS 5 and the Holocene. Similarly, PR-LA-1 shows decreasing amplitudes of
527 centennial to millennial oscillations after 30 ka compared to NGRIP and Cariaco with weak or
528 even absent excursions across GIs 2 to 5 (Figure 5). Oster et al. (2019) identified an east–west
529 gradient in precipitation patterns based on late Holocene speleothem $\delta^{18}O$ records, with
530 increasing Pacific influence when moving across the Caribbean towards the west. As the
531 northern extent of the ITCZ moves further south, it causes a progressive weakening of the
532 connection between Caribbean precipitation and North Atlantic forcing and affects the
533 competing influence of the Atlantic and Pacific. This is also a likely explanation for the
534 observed patterns in the Caribbean precipitation records on centennial to millennial scale during
535 the last glacial period, highlighting the complex climatological patterns in this region.

536 ## 5 Conclusions

537 The speleothem multi-proxy record from Larga Cave provides valuable insights into regional
538 paleoclimate variability on multi-decadal to orbital timescales, whereby $\delta^{18}O$ values are the key
539 proxy of past precipitation amount. This study highlights the close connection of western
540 tropical Atlantic precipitation variability and Northern Hemisphere climate variability on
541 millennial to centennial timescales. In particular, our record underlines the central and persistent
542 role of the strength of the AMOC for abrupt glacial climate change, adding valuable information
543 to recent debates and underscoring that a more complete understanding of the underlying
544 mechanisms can only be achieved by integrating observations and models (Roberts & Hopcroft,
545 2020; Them Il et al., 2015). The compilation of regional records from speleothems and other
546 archives suggests the existence of spatially and temporally varying precipitation patterns during
547 the last glacial period. These observations argue for a complex ITCZ variability, with
548 meridional shifts occurring along with expansions and contractions of the rain belt on different
549 timescales and depending on the nature of the forcing. Thus, the concept of north-south shifts
550 of the ITCZ causing wet-dry conditions in the region is insufficient to explain the observed
551 tropical precipitation variability and requires further in-depth research on the variability and

drivers of the western tropical Atlantic rain belt. As shown in this study, precisely dated speleothem records can provide important information towards this endeavour.

Acknowledgements

S.W., D.S. and A.M. acknowledge funding by DFG grants MA 821/37-2, SCHO 1274/6-1, SCHO 1274/9-1, and SCHO 1274/11-1. Special thanks go to J. Estrella, F. Sperberg and J. Santiago from the University of Puerto Rico (Mayagüez) and J. Dutil, J. Kruse, T. Rowe, A. Castro and J. Scheer for their outstanding support in the field. We thank F. Rodriguez-Morales and his family for their long term support. The authors also thank the staff of Empresas Gallo, Carolina, Puerto Rico, for support with sample preparation as well as B. Stoll, U. Weis, B. Schwager and M. Wimmer for assistance in the laboratories. N. Frank is thanked for support and helpful comments to this manuscript.

Data availability

The data presented in this paper were uploaded to the open PANGAEA data library (https://doi.pangaea.de/10.1594/PANGAEA.911486) and will be available after acceptance of this paper.

Supporting information

Supporting information S1: Simulation of the observed proxy variability.
Table S 1: Results of the linear fit models for each Osmond isochron indicated in Figure S 2.
Table S 2: Activity ratios and final ages of stalagmite PR-LA-1.
Figure S 1 Map of Larga Cave and location of stalagmite PR-LA-1, Puerto Rico
Figure S 2: Individual Osmond type I isochrones and ($^{230}Th/^{238}U$) vs. ($^{232}Th/^{238}U$) activity ratios of stalagmite PR-LA-1.
Figure S 3: Results of I-STAL simulations for speleothem PR-LA-1 compared to speleothem proxies.
Figure S 4: ISOLUTION simulations of the stable isotopic composition of calcite.
Figure S 5: Spectral power for different intervals of the PR-LA-1 $\delta^{13}C$ record**.**
Figure S 6: Spectral power for different intervals of the PR-LA-1 Mg/Ca record.

References

Arienzo, M. M., Swart, P. K., Broad, K., Clement, A. C., Pourmand, A., & Kakuk, B. (2017). Multi-proxy evidence of millennial climate variability from multiple Bahamian speleothems. *Quaternary Science Reviews, 161*, 18-29. doi:10.1016/j.quascirev.2017.02.004

Arienzo, M. M., Swart, P. K., Pourmand, A., Broad, K., Clement, A. C., Murphy, L. N., et al. (2015). Bahamian speleothem reveals temperature decrease associated with Heinrich stadials. *Earth and Planetary Science Letters, 430*, 377-386. doi:10.1016/j.epsl.2015.08.035

Asmerom, Y., Baldini, J. U., Prufer, K. M., Polyak, V. J., Ridley, H. E., Aquino, V. V., et al. (2020). Intertropical convergence zone variability in the Neotropics during the Common Era. *Science Advances, 6*(7), eaax3644.

Baker, A. J., Mattey, D. P., & Baldini, J. U. L. (2014). Reconstructing modern stalagmite growth from cave monitoring, local meteorology, and experimental measurements of dripwater films. *Earth and Planetary Science Letters, 392*, 239-249.

Baker, P. A., & Fritz, S. C. (2015). Nature and causes of Quaternary climate variation of tropical South America. *Quaternary Science Reviews, 124*, 31-47.

Beck, J. W., Richards, D. A., Edwards, R. L., Silverman, B. W., Smart, P. L., Donahue, D. J., et al. (2001). Extremely large variations of atmospheric 14C concentration during the last glacial period. *Science, 292*(5526), 2453-2458. doi:10.1126/science.1056649

Bhattacharya, T., Chiang, J. C., & Cheng, W. (2017). Ocean-atmosphere dynamics linked to 800–1050 CE drying in mesoamerica. *Quaternary Science Reviews, 169*, 263-277.

Böhm, E., Lippold, J., Gutjahr, M., Frank, M., Blaser, P., Antz, B., et al. (2015). Strong and deep Atlantic meridional overturning circulation during the last glacial cycle. *Nature, 517*(7532), 73-76. doi:10.1038/nature14059

Broccoli, A. J., Dahl, K. A., & Stouffer, R. J. (2006). Response of the ITCZ to Northern Hemisphere cooling. *Geophysical Research Letters, 33*(1), n/a-n/a. doi:10.1029/2005gl024546

Burckel, P., Waelbroeck, C., Gherardi, J. M., Pichat, S., Arz, H., Lippold, J., et al. (2015). Atlantic Ocean circulation changes preceded millennial tropical South America rainfall events during the last glacial. *Geophysical Research Letters, 42*(2), 411-418. doi:10.1002/2014gl062512

Cheng, H., Edwards, R. L., Hoff, J., Gallup, C. D., Richards, D. A., & Asmerom, Y. (2000). The half-lives of uranium-234 and thorium-230. *Chemical Geology, 169*(1-2), 17-33. doi:10.1016/s0009-2541(99)00157-6

Clark, P. U., Marshall, S. J., Clarke, G. K., Hostetler, S. W., Licciardi, J. M., & Teller, J. T. (2001). Freshwater forcing of abrupt climate change during the last glaciation. *Science, 293*(5528), 283-287.

618 Correa-Metrio, A., Bush, M. B., Cabrera, K. R., Sully, S., Brenner, M., Hodell, D. A., et al.
619 (2012). Rapid climate change and no-analog vegetation in lowland Central America
620 during the last 86,000 years. *Quaternary Science Reviews, 38*, 63-75.
621 doi:10.1016/j.quascirev.2012.01.025
622 Cruz, F. W., Burns, S. J., Jercinovic, M., Karmann, I., Sharp, W. D., & Vuille, M. (2007).
623 Evidence of rainfall variations in Southern Brazil from trace element ratios (Mg/Ca and
624 Sr/Ca) in a Late Pleistocene stalagmite. *Geochimica et Cosmochimica Acta, 71*(9),
625 2250-2263. doi:10.1016/j.gca.2007.02.005
626 Cruz, F. W., Wang, X., Auler, A., Vuille, M., Burns, S. J., Edwards, L. R., et al. (2009). Orbital
627 and millennial-scale precipitation changes in Brazil from speleothem records. In *Past*
628 *Climate Variability in South America and Surrounding Regions* (pp. 29-60): Springer.
629 Deininger, M., & Scholz, D. (2019). ISOLUTION 1.0: an ISOtope evoLUTION model
630 describing the stable oxygen (δ 18 O) and carbon (δ 13 C) isotope values of speleothems.
631 *International Journal of Speleology, 48*(1), 3.
632 del Monte-Luna, P., Villalobos, H., & Arreguín-Sánchez, F. (2015). Variability of sea surface
633 temperature in the southwestern Gulf of Mexico. *Continental Shelf Research, 102*, 73-
634 79.
635 Deplazes, G., Lückge, A., Peterson, L. C., Timmermann, A., Hamann, Y., Hughen, K. A., et al.
636 (2013). Links between tropical rainfall and North Atlantic climate during the last glacial
637 period. *Nature Geoscience, 6*(3), 213-217.
638 Dreybrodt, W., & Scholz, D. (2011). Climatic dependence of stable carbon and oxygen isotope
639 signals recorded in speleothems: From soil water to speleothem calcite. *Geochimica et*
640 *Cosmochimica Acta, 75*(3), 734-752. doi:10.1016/j.gca.2010.11.002
641 Enfield, D. B., Mestas-Nuñez, A. M., & Trimble, P. J. (2001). The Atlantic multidecadal
642 oscillation and its relation to rainfall and river flows in the continental US. *Geophysical*
643 *Research Letters, 28*(10), 2077-2080.
644 Escobar, J., Hodell, D. A., Brenner, M., Curtis, J. H., Gilli, A., Mueller, A. D., et al. (2012). A
645 ~43-ka record of paleoenvironmental change in the Central American lowlands inferred
646 from stable isotopes of lacustrine ostracods. *Quaternary Science Reviews, 37*, 92-104.
647 doi:10.1016/j.quascirev.2012.01.020
648 Fensterer, C., Scholz, D., Hoffmann, D., Mangini, A., & Pajón, J. M. (2010). 230Th/U-dating
649 of a late Holocene low uranium speleothem from Cuba. *IOP Conference Series: Earth*
650 *and Environmental Science, 9*, 012015. doi:10.1088/1755-1315/9/1/012015
651 Fensterer, C., Scholz, D., Hoffmann, D., Spötl, C., Pajón, J. M., & Mangini, A. (2012). Cuban
652 stalagmite suggests relationship between Caribbean precipitation and the Atlantic
653 Multidecadal Oscillation during the past 1.3 ka. *The Holocene*, 0959683612449759.
654 Fensterer, C., Scholz, D., Hoffmann, D. L., Spötl, C., Schröder-Ritzrau, A., Horn, C., et al.
655 (2013). Millennial-scale climate variability during the last 12.5 ka recorded in a
656 Caribbean speleothem. *Earth and Planetary Science Letters, 361*, 143-151.
657 Granger, O. E. (1985). Caribbean climates. *Progress in Physical Geography, 9*(1), 16-43.

Hagen, S., & Keigwin, L. D. (2002). Sea-surface temperature variability and deep water reorganisation in the subtropical North Atlantic during Isotope Stage 2--4. *Marine Geology, 189*(1), 145-162.

Hansen, M., Scholz, D., Schöne, B. R., & Spötl, C. (2019). Simulating speleothem growth in the laboratory: Determination of the stable isotope fractionation (δ13C and δ18O) between H2O, DIC and CaCO3. *Chemical Geology, 509*, 20-44.

Hellstrom, J. (2006). U–Th dating of speleothems with high initial 230Th using stratigraphical constraint. *Quaternary Geochronology, 1*(4), 289-295. doi:10.1016/j.quageo.2007.01.004

Henry, L., McManus, J. F., Curry, W. B., Roberts, N. L., Piotrowski, A. M., & Keigwin, L. D. (2016). North Atlantic ocean circulation and abrupt climate change during the last glaciation. *Science, 353*(6298), 470-474.

Hodell, D. A., Anselmetti, F. S., Ariztegui, D., Brenner, M., Curtis, J. H., Gilli, A., et al. (2008). An 85-ka record of climate change in lowland Central America. *Quaternary Science Reviews, 27*(11-12), 1152-1165. doi:10.1016/j.quascirev.2008.02.008

Jochum, K. P., Scholz, D., Stoll, B., Weis, U., Wilson, S. A., Yang, Q., et al. (2012). Accurate trace element analysis of speleothems and biogenic calcium carbonates by LA-ICP-MS. *Chemical Geology, 318-319*, 31-44. doi:10.1016/j.chemgeo.2012.05.009

Jochum, K. P., Weis, U., Stoll, B., Kuzmin, D., Yang, Q., Raczek, I., et al. (2011). Determination of Reference Values for NIST SRM 610-617 Glasses Following ISO Guidelines. *Geostandards and Geoanalytical Research, 35*(4), 397-429. doi:10.1111/j.1751-908X.2011.00120.x

Lachniet, M. S., Asmerom, Y., Bernal, J. P., Polyak, V. J., & Vazquez-Selem, L. (2013). Orbital pacing and ocean circulation-induced collapses of the Mesoamerican monsoon over the past 22,000 y. *Proceedings of the National Academy of Sciences, 110*(23), 9255-9260. doi:10.1073/pnas.1222804110

Lachniet, M. S., Johnson, L., Asmerom, Y., Burns, S. J., Polyak, V., Patterson, W. P., et al. (2009). Late Quaternary moisture export across Central America and to Greenland: evidence for tropical rainfall variability from Costa Rican stalagmites. *Quaternary Science Reviews, 28*(27-28), 3348-3360. doi:10.1016/j.quascirev.2009.09.018

Lea, D. W., Pak, D. K., Peterson, L. C., & Hughen, K. A. (2003). Synchroneity of tropical and high-latitude Atlantic temperatures over the last glacial termination. *Science, 301*(5638), 1361-1364. doi:10.1126/science.1088470

Lippold, J., Grützner, J., Winter, D., Lahaye, Y., Mangini, A., & Christl, M. (2009). Does sedimentary 231Pa/230Th from the Bermuda Rise monitor past Atlantic meridional overturning circulation? *Geophysical Research Letters, 36*(12).

Lippold, J., Pöppelmeier, F., Süfke, F., Gutjahr, M., Goepfert, T. J., Blaser, P., et al. (2019). Constraining the variability of the atlantic meridional overturning circulation during the holocene. *Geophysical Research Letters, 46*(20), 11338-11346.

Ludwig, K. R., & Titterington, D. (1994). Calculation of 230ThU isochrons, ages, and errors. *Geochimica et Cosmochimica Acta, 58*(22), 5031-5042.

Lynch-Stieglitz, J., Schmidt, M. W., Henry, L. G., Curry, W. B., Skinner, L. C., Mulitza, S., et al. (2014). Muted change in Atlantic overturning circulation over some glacial-aged Heinrich events. *Nature Geoscience, 7*(2), 144-150. doi:10.1038/Ngeo2045

Mattey, D., Fairchild, I., Atkinson, T., Latin, J., Ainsworth, M., & Durell, R. (2010). Gibraltar and trace elements in modern speleothem from St Michaels Cave, Seasonal microclimate control of calcite fabrics, stable isotopes. *Tufas and Speleothems: Unravelling the Microbial and Physical Controls, 336*, 323-344.

McManus, J. F., Francois, R., Gherardi, J. M., Keigwin, L. D., & Brown-Leger, S. (2004). Collapse and rapid resumption of Atlantic meridional circulation linked to deglacial climate changes. *Nature, 428*(6985), 834-837. doi:10.1038/nature02494

Medina-Elizalde, M., Burns, S. J., Lea, D. W., Asmerom, Y., von Gunten, L., Polyak, V., et al. (2010). High resolution stalagmite climate record from the Yucatán Peninsula spanning the Maya terminal classic period. *Earth and Planetary Science Letters, 298*(1-2), 255-262. doi:10.1016/j.epsl.2010.08.016

Medina-Elizalde, M., Burns, S. J., Polanco-Martinez, J., Lases-Hernández, F., Bradley, R., Wang, H.-C., et al. (2017). Synchronous precipitation reduction in the American Tropics associated with Heinrich 2. *Scientific reports, 7*(1), 11216.

Obert, J. C., Scholz, D., Felis, T., Brocas, W. M., Jochum, K. P., & Andreae, M. O. (2016). 230Th/U dating of Last Interglacial brain corals from Bonaire (southern Caribbean) using bulk and theca wall material. *Geochimica et Cosmochimica Acta, 178*, 20-40. doi:10.1016/j.gca.2016.01.011

Oster, J. L., Warken, S. F., Sekhon, N., Arienzo, M. M., & Lachniet, M. (2019). Speleothem Paleoclimatology for the Caribbean, Central America, and North America. *Quaternary, 2*(1), 5.

Peterson, L. C., Haug, G. H., Hughen, K. A., & Rohl, U. (2000). Rapid changes in the hydrologic cycle of the tropical Atlantic during the last glacial. *Science, 290*(5498), 1947-1951. doi:10.1126/science.290.5498.1947

Poveda, G., Waylen, P. R., & Pulwarty, R. S. (2006). Annual and inter-annual variability of the present climate in northern South America and southern Mesoamerica. *Palaeogeography Palaeoclimatology Palaeoecology, 234*(1), 3-27. doi:10.1016/j.palaeo.2005.10.031

Rasmussen, S. O., Bigler, M., Blockley, S. P., Blunier, T., Buchardt, S. L., Clausen, H. B., et al. (2014). A stratigraphic framework for abrupt climatic changes during the Last Glacial period based on three synchronized Greenland ice-core records: refining and extending the INTIMATE event stratigraphy. *Quaternary Science Reviews, 106*, 14-28.

Rivera-Collazo, I., Winter, A., Scholz, D., Mangini, A., Miller, T., Kushnir, Y., et al. (2015). Human adaptation strategies to abrupt climate change in Puerto Rico ca. 3.5 ka. *The Holocene, 25*(4), 627-640. doi:10.1177/0959683614565951

737 Roberts, W., & Hopcroft, P. (2020). Controls on the tropical response to abrupt climate changes.
738 *Geophysical Research Letters*, e2020GL087518.
739 Schellekens, J., Scatena, F., Bruijnzeel, L., Van Dijk, A., Groen, M., & Van Hogezand, R.
740 (2004). Stormflow generation in a small rainforest catchment in the Luquillo
741 Experimental Forest, Puerto Rico. *Hydrological Processes, 18*(3), 505-530.
742 Schmidt, M. W., & Spero, H. J. (2011). Meridional shifts in the marine ITCZ and the tropical
743 hydrologic cycle over the last three glacial cycles. *Paleoceanography, 26*(1).
744 doi:10.1029/2010pa001976
745 Schmidt, M. W., Spero, H. J., & Lea, D. W. (2004). Links between salinity variation in the
746 Caribbean and North Atlantic thermohaline circulation. *Nature, 428*(6979), 160-163.
747 doi:10.1038/nature02346
748 Scholz, D., & Hoffmann, D. L. (2011). StalAge – An algorithm designed for construction of
749 speleothem age models. *Quaternary Geochronology, 6*(3-4), 369-382.
750 doi:10.1016/j.quageo.2011.02.002
751 Schulz, M., & Mudelsee, M. (2002). REDFIT: estimating red-noise spectra directly from
752 unevenly spaced paleoclimatic time series. *Computers & Geosciences, 28*(3), 421-426.
753 Sinclair, D. J., Banner, J. L., Taylor, F. W., Partin, J., Jenson, J., Mylroie, J., et al. (2012).
754 Magnesium and strontium systematics in tropical speleothems from the Western Pacific.
755 *Chemical Geology, 294*, 1-17. doi:10.1016/j.chemgeo.2011.10.008
756 Singarayer, J. S., Valdes, P. J., & Roberts, W. H. G. (2017). Ocean dominated expansion and
757 contraction of the late Quaternary tropical rainbelt. *Scientific reports, 7*(1), 9382.
758 doi:10.1038/s41598-017-09816-8
759 Spötl, C. (2011). Long-term performance of the Gasbench isotope ratio mass spectrometry
760 system for the stable isotope analysis of carbonate microsamples. *Rapid Commun Mass*
761 *Spectrom, 25*(11), 1683-1685. doi:10.1002/rcm.5037
762 Spötl, C., & Vennemann, T. W. (2003). Continuous-flow isotope ratio mass spectrometric
763 analysis of carbonate minerals. *Rapid Commun Mass Spectrom, 17*(9), 1004-1006.
764 doi:10.1002/rcm.1010
765 Stoll, H. M., Müller, W., & Prieto, M. (2012). I-STAL, a model for interpretation of Mg/Ca,
766 Sr/Ca and Ba/Ca variations in speleothems and its forward and inverse application on
767 seasonal to millennial scales. *Geochemistry, Geophysics, Geosystems, 13*(9).
768 doi:10.1029/2012gc004183
769 Stríkis, N. M., Chiessi, C. M., Cruz, F. W., Vuille, M., Cheng, H., de Souza Barreto, E. A., et
770 al. (2015). Timing and structure of Mega-SACZ events during Heinrich Stadial 1.
771 *Geophysical Research Letters, 42*(13), 5477-5484A.
772 Svensson, A., Andersen, K. K., Bigler, M., Clausen, H. B., Dahl-Jensen, D., Davies, S. M., et
773 al. (2008). A 60 000 year Greenland stratigraphic ice core chronology. *Climate of the*
774 *Past, 4*(1), 47-57.
775 Them Il, T. R., Schmidt, M. W., & Lynch-Stieglitz, J. (2015). Millennial-scale tropical
776 atmospheric and Atlantic Ocean circulation change from the Last Glacial Maximum and

Marine Isotope Stage 3. *Earth and Planetary Science Letters, 427*, 47-56. doi:10.1016/j.epsl.2015.06.062

Ting, M., Kushnir, Y., Seager, R., & Li, C. (2009). Forced and internal twentieth-century SST trends in the North Atlantic. *Journal of Climate, 22*(6), 1469-1481.

Tremaine, D. M., Froelich, P. N., & Wang, Y. (2011). Speleothem calcite farmed in situ: modern calibration of δ18O and δ13C paleoclimate proxies in a continuously-monitored natural cave system. *Geochimica et Cosmochimica Acta, 75*(17), 4929-4950.

Vieten, R., Warken, S., Winter, A., Scholz, D., Miller, T., Spötl, C., et al. (2018a). Monitoring of Cueva Larga, Puerto Rico—A First Step to Decode Speleothem Climate Records. In W. B. White, J. S. Herman, E. K. Herman, & M. Rutigliano (Eds.), *Karst Groundwater Contamination and Public Health* (pp. 319-331). Cham: Springer International Publishing.

Vieten, R., Warken, S., Winter, A., Schröder-Ritzrau, A., Scholz, D., & Spötl, C. (2018b). Hurricane Impact on Seepage Water in Larga Cave, Puerto Rico. *Journal of Geophysical Research-Biogeosciences, 123*(3), 879-888. doi:10.1002/2017jg004218

Vieten, R., Winter, A., Warken, S. F., Schröder-Ritzrau, A., Miller, T. E., & Scholz, D. (2016). Seasonal temperature variations controlling cave ventilation processes in Cueva Larga, Puerto Rico. *International Journal of Speleology, 45*(3), 259-273. doi:10.5038/1827-806x.45.3.1983

Waelbroeck, C., Pichat, S., Böhm, E., Lougheed, B. C., Faranda, D., Vrac, M., et al. (2018). Relative timing of precipitation and ocean circulation changes in the western equatorial Atlantic over the last 45 kyr. *Clim. Past, 14*(9), 1315-1330. doi:10.5194/cp-14-1315-2018

Warken, S. F., Fohlmeister, J., Schröder-Ritzrau, A., Constantin, S., Spotl, C., Gerdes, A., et al. (2018). Reconstruction of late Holocene autumn/winter precipitation variability in SW Romania from a high-resolution speleothem trace element record. *Earth and Planetary Science Letters, 499*, 122-133. doi:10.1016/j.epsl.2018.07.027

Warken, S. F., Scholz, D., Spötl, C., Jochum, K. P., Pajón, J. M., Bahr, A., et al. (2019). Caribbean hydroclimate and vegetation history across the last glacial period. *Quaternary Science Reviews, 218*, 75-90.

Wassenburg, J. A., Riechelmann, S., Schröder-Ritzrau, A., Riechelmann, D. F. C., Richter, D. K., Immenhauser, A., et al. (2019). Calcite Mg and Sr partition coefficients in cave environments: implications for interpreting prior calcite precipitation in speleothems. *Geochimica et Cosmochimica Acta*. doi:https://doi.org/10.1016/j.gca.2019.11.011

Wedepohl, K. H. (1995). The Composition of the Continental-Crust. *Geochimica et Cosmochimica Acta, 59*(7), 1217-1232.

Wenz, S., Scholz, D., Sürmelihindi, G., Passchier, C. W., Jochum, K. P., & Andreae, M. O. (2016). 230Th/U-dating of carbonate deposits from ancient aqueducts. *Quaternary Geochronology, 32*, 40-52. doi:10.1016/j.quageo.2015.12.001

Winter, A., Miller, T., Kushnir, Y., Sinha, A., Timmermann, A., Jury, M. R., et al. (2011). Evidence for 800years of North Atlantic multi-decadal variability from a Puerto Rican speleothem. *Earth and Planetary Science Letters, 308*(1-2), 23-28. doi:10.1016/j.epsl.2011.05.028

Winter, A., Zanchettin, D., Lachniet, M., Vieten, R., Pausata, F. S. R., Ljungqvist, F. C., et al. (2020). Initiation of a stable convective hydroclimatic regime in Central America circa 9000 years BP. *Nature Communications, 11*(1), 716. doi:10.1038/s41467-020-14490-y

Yang, Q., Scholz, D., Jochum, K. P., Hoffmann, D. L., Stoll, B., Weis, U., et al. (2015). Lead isotope variability in speleothems—A promising new proxy for hydrological change? First results from a stalagmite from western Germany. *Chemical Geology, 396*, 143-151. doi:10.1016/j.chemgeo.2014.12.028

Zanchettin, D., Bothe, O., Müller, W., Bader, J., & Jungclaus, J. H. (2014). Different flavors of the Atlantic multidecadal variability. *Climate Dynamics, 42*(1-2), 381-399.

Zhang, J., & Zhang, R. (2015). On the evolution of Atlantic meridional overturning circulation fingerprint and implications for decadal predictability in the North Atlantic. *Geophysical Research Letters, 42*(13), 5419-5426.

Paleoceanography and Paleoclimatology

Supporting Information for

Persistent link between Caribbean precipitation and Atlantic Ocean circulation during the Last Glacial revealed by a speleothem record from Puerto Rico

Sophie F. Warken[1,2,3*], Rolf Vieten[4], Amos Winter[4,5], Christoph Spötl[6], Thomas E. Miller[7], Klaus P. Jochum[8], Andrea Schröder-Ritzrau[2], Augusto Mangini[2], and Denis Scholz[1]

[1] Institute for Geosciences, University of Mainz, Germany; [2] Institute of Environmental Physics, University of Heidelberg, Germany; [3] Institute of Earth Sciences, Heidelberg University, Germany; [4] Department of Marine Sciences, University of Puerto Rico, Mayagüez, Puerto Rico [5] Earth and Environmental Systems Department, Indiana State University, Terre Haute, Indiana, USA [6] Institute of Geology, University of Innsbruck, Austria; [7] Department of Geology, University of Puerto Rico, Mayagüez, Puerto Rico; [8] Max Planck Institute for Chemistry, Climate Geochemistry Department, Mainz, Germany

Contents of this file

Additional Supporting Information (Files uploaded separately)

Introduction

This supporting material contains several parts. Figure S 1 is a map of Larga Cave and indicates the location of stalagmite PR-LA-1. We also present additional information on the chronology of speleothem PR-LA-1, i.e., the results of the linear fits for each Osmond isochron (Table S 1 and Figure S 2) as well as the activity ratios and calculated ages of stalagmite PR-LA-1 (Table S 2, uploaded as separate file). In addition, results and discussion of the numerical simulations of the observed proxy variability using I-STAL (Stoll et al., 2012), ISOLUTION 1.0 (Deininger & Scholz, 2019) and REDFIT (Schulz & Mudelsee, 2002) are included. The supporting text S1 as well as Figures S3 and S4 show the results of the proxy process simulations. Figures S5 and S6 indicate the spectral power distributions for different intervals of the PR-LA-1 $\delta^{13}C$ and Mg/Ca records.

Figure S1. Map of Larga cave and location of stalagmite PR-LA-1, Puerto Rico (red symbol). The sample was collected from the main passage. After Miller (2010).

35

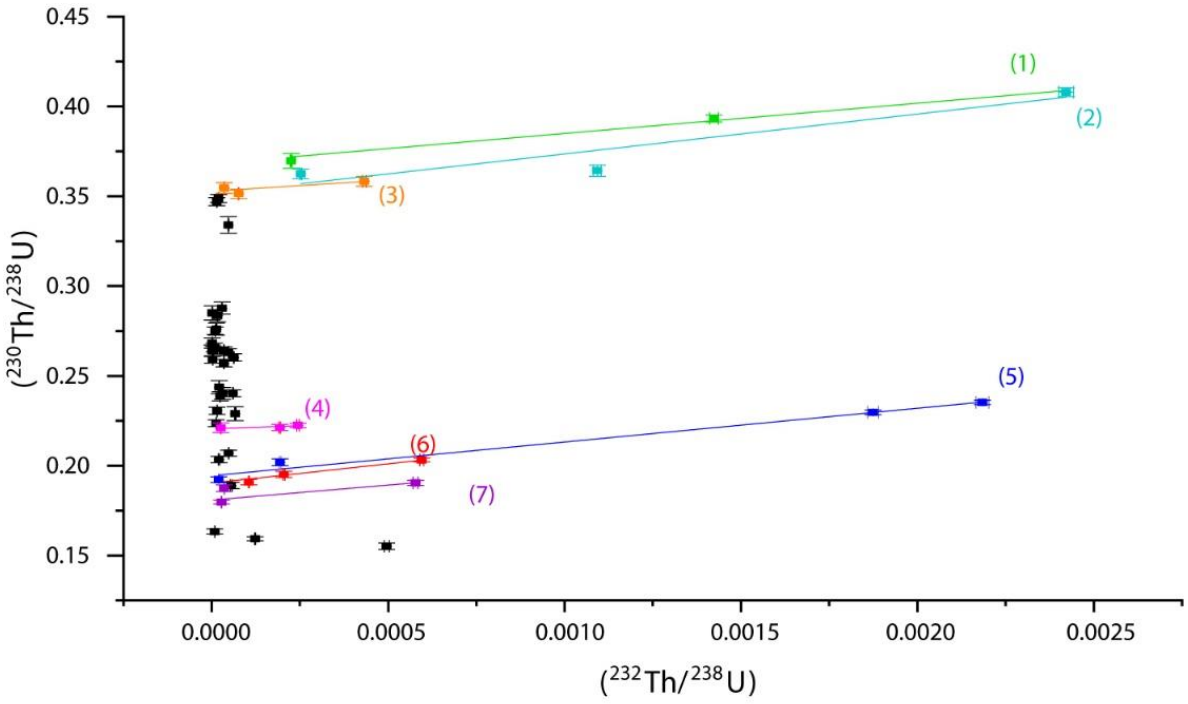

40 **Figure S2. Measured ($^{230}Th/^{238}U$) vs. ($^{232}Th/^{238}U$) activity ratios in stalagmite PR-LA-1. Different colours correspond to the individual Osmond type I isochrons and data points (Table S1).**

Table S1. Results of the linear fits for each Osmond isochron shown in Figure S 2.

# Isochron	Slope	Error	Pearson's r	N
1	16.81	± 2.08	0.99	3
2	22.22	± 7.23	0.93	3
3	12.38	± 6.70	0.85	5
4	7.04	± 14.02	0.72	3
5	18.78	± 1.42	0.99	4
6	21.35	± 2.90	0.97	4
7	16.67	± 10.64	0.72	3
Overall mean:	**16.46**	**10.58**		
For r > 0.9	**19.79**	**4.93**		

Table S2 (uploaded separately). Activity ratios and calculated ages of stalagmite PR-LA-1. Activity ratios corrected for initial Th assuming an detrital weight ratio $^{232}Th/^{238}U$ = 0.154 ± 0.038 (corresponding to an activity ratio of the detritus in secular equilibrium of $(^{230}Th/^{232}Th)_{detr}$ = 19.79 ± 4.93). Ages are calculated using the decay constants of Cheng et al. (2000). Uncertainties are given at the 2σ-level, and do not include half-life uncertainties.

Text S1. Simulation of the observed proxy variability

Inverse modelling of elemental variations using I-STAL

In order to explore drivers of trace element variability in PR-LA-1, the inverse model I-STAL was applied, similarly as described in Stoll et al. (2012). To evaluate changes on centennial to millennial timescales, the records of Mg/Ca, Sr/Ca and Ba/Ca were reduced to 100-year average values. The choice of model input parameters is closely oriented on observed variations during the cave monitoring and in the speleothem. The recorded increase of element to calcium ratios towards 15.4 ka gives the order of magnitude of the degree of enrichment by PCP of Mg, Sr and Ba, which is set to a factor of 5 (Mg), 2 (Sr) and 3 (Ba), respectively. Ca concentrations at drip sites in Larga Cave today are between 50 to 75 ppm. The range for drip intervals was set to 1 to 5000 s. We suggest that the strongest enrichment due to PCP occurs for extremely low flow, so the drip interval of maximum water-rock exchange is set to 5000 s. Cave temperature was set to 20°C, accounting for the observed mean temperature difference between the Holocene and the LGM in the region (e.g., Arienzo et al. (2015); Lea et al. (2003)).

In a first simulation, initial Ca was set to 50 ppm, and the model was run to optimize for drip interval and pCO_2. In the next step, unphysically low cave air pCO_2 values of less than atmospheric pCO_2 during the Last Glacial were set to this lower limit of 180 ppm, and the model was run to optimize for drip interval and initial Ca. This simulation was repeated for different parametrizations of e.g., baseline of initial Ca, maximum drip interval or the degree of enrichment by PCP. However, despite small absolute shifts in the mean values, the temporal variability of the modelled drip intervals and the degree of supersaturation remained relatively unaffected by the choice of variables and is therefore here only displayed for an example set of input parameters (Figure S 4). A second run first optimizing drip interval and initial Ca, and in a second step pCO_2 led to similar results. The modelled drip intervals vary over 5 orders of magnitude between 1 and 10000 s, whereas highest drip intervals were reached in the last phase of the record after 17.5 ka. In the same period, calcite supersaturation is at its lowest values.

All simulations modelled stalagmite Sr/Ca and Mg/Ca ratios well, while Ba/Ca variations are poorly reproduced. Average simulated growth rates are in the range of values as suggested by the age model (10 to 1000 µm/a).

Sensitivity simulation of processes influencing speleothem stable isotope composition

The range of the main parameters simulated by I-STAL was selected to evaluate the influence of temperature, drip interval and state of supersaturation on the speleothem $\delta^{18}O$ and $\delta^{13}C$ values using ISOLUTION 1.0 (Deininger & Scholz, 2019) and the isotopic fractionation factor of Tremaine et al. (2011). Unless stated otherwise, cave temperature was set to 20°C, drip water pCO_2 to 5000 ppm, cave air pCO_2 to 300ppmv, relative humidity (rH) to 99%, wind speed to 0 m/s and the mixing parameter Φ to 1. In agreement with the monitoring results, drip water $\delta^{18}O$ and $\delta^{13}C$ values were set to -2.6 and -13‰, respectively. Figure A2 shows that, keeping all other parameters constant, speleothem $\delta^{18}O$ and $\delta^{13}C$ values increase with the drip interval and the degree of supersaturation of the drip water, reaching a maximum isotope fractionation of the calcite up to +1.5‰ ($\delta^{18}O$) and 1.2‰ ($\delta^{13}C$) compared to equilibrium conditions.

While temperature has only a small impact on carbon isotope fractionation, a decrease in cave air temperature by 5°C may account for a +1‰ increase in $\delta^{18}O$ values. Evaporation effects can strongly influence the isotopic composition of the calcite. However, at high drip rates, already a moderate reduction of rH by 5% would lead to an increase of more than +1‰ in $\delta^{18}O$ and +2‰ in $\delta^{13}C$.

Combining all these effects, leads to $\delta^{18}O$ values of the calcite between -1.6 and -1.1‰ for a drip interval of 10,000s, T = 17.5°C, rH = 90% and drip water pCO_2 values of 975 and 3000ppmv, corresponding to initial Ca concentrations of 30 and 50 ppm, respectively. A temperature decrease of 15°C would further increase this value to -0.7‰. $\delta^{13}C$ values increase to a maximum of -11‰ in these

scenarios. Under these extreme conditions, the highest measured values in the speleothem of +2‰ ($\delta^{18}O$) and -4‰ ($\delta^{13}C$) can only be reproduced with drip water values of about 0‰ for $\delta^{18}O$ and -6‰ for $\delta^{13}C$, respectively.

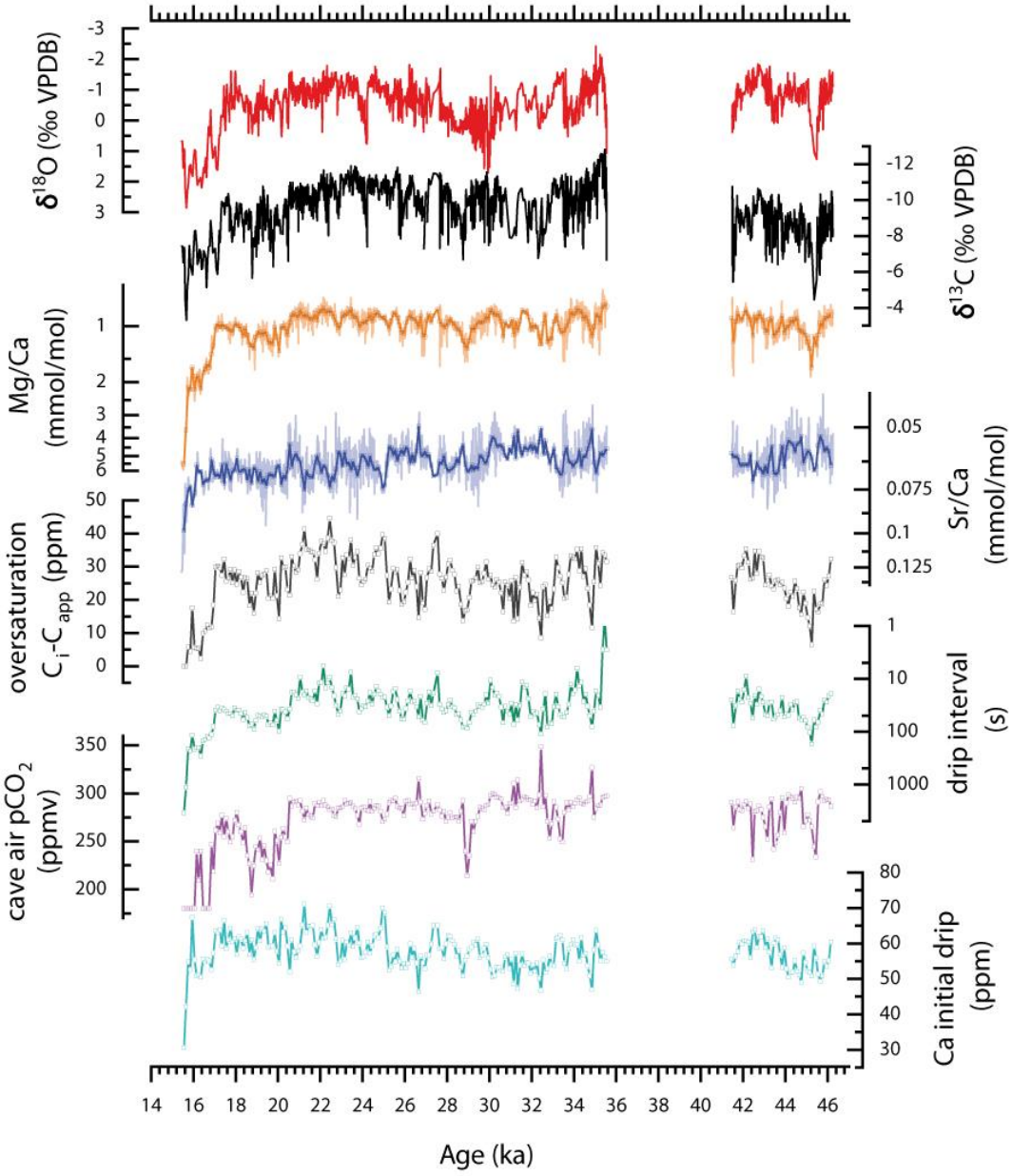

Figure S3. Results of I-STAL simulations for speleothem PR-LA-1 compared to speleothem proxies. Top panels: stable isotopes of oxygen ($\delta^{18}O$ in ‰ (red) and carbon ($\delta^{13}C$ in ‰, black), molar trace element to calcium ratios: Mg/Ca (orange), Sr/Ca (blue). Light coloured lines are the raw speleothem data, dark coloured lines interpolated to 100 y average values. Open symbols indicate modelled Mg/Ca and Sr/Ca ratios. Bottom panels: calculated oversaturation of the drip (grey), drip interval (green), cave air pCO_2 (purple) and initial Ca concentration of the drip water (turquoise).

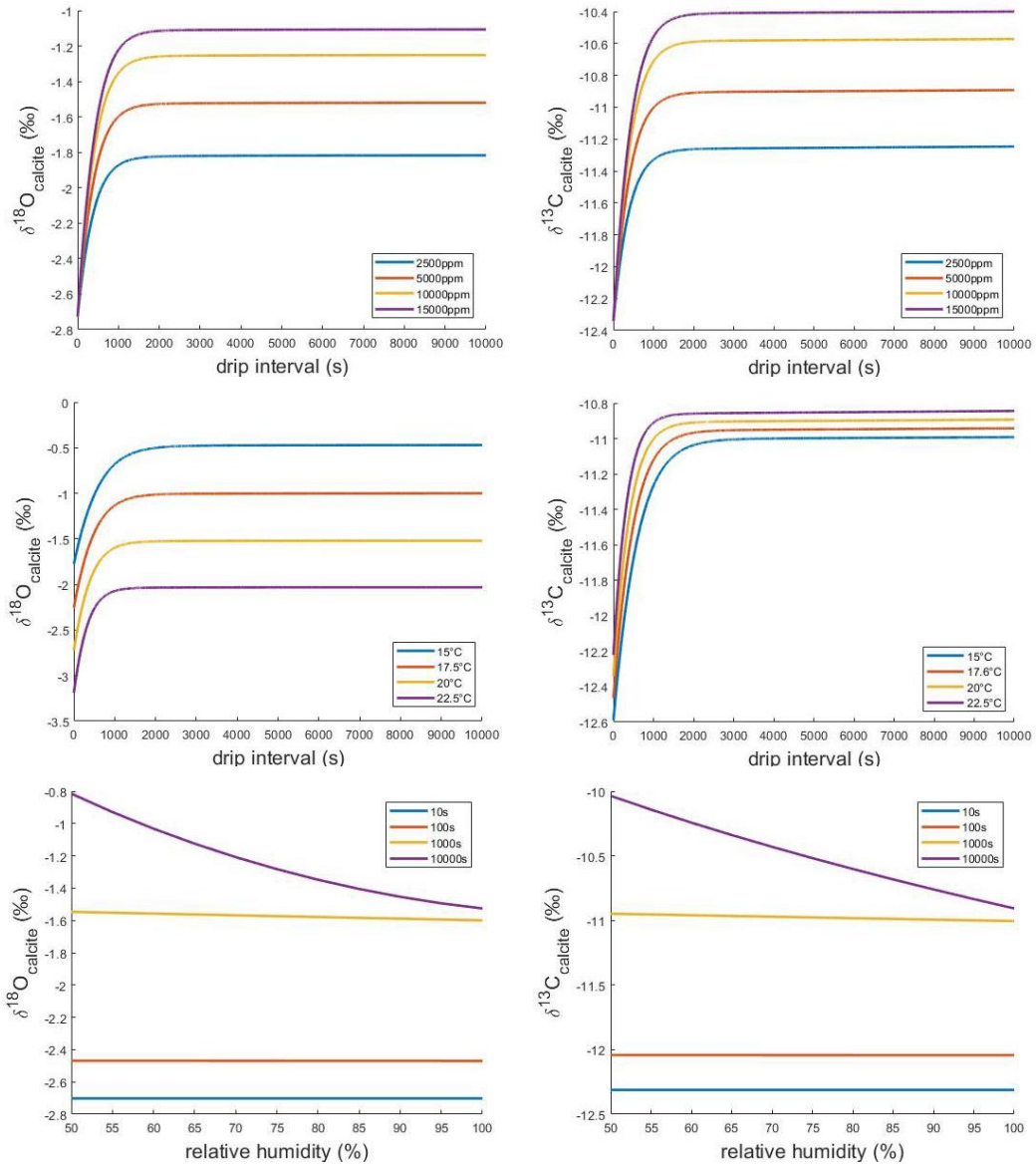

Figure S4. Simulations of the stable isotopic composition of calcite assuming initial drip water values of $\delta^{18}O$ of -2.6‰ (VSMOW) and $\delta^{13}C$ of -13 ‰. Unless stated otherwise in the individual plots, cave temperature was set to 20°C, drip water pCO_2 to 5000ppm, cave air pCO_2 to 300ppmv, relative humidity to 99%, wind speed to 0 m/s and the mixing parameter Φ to 1. All simulations calculated with ISOLUTION 1.0 (Deininger & Scholz, 2019), assuming a temperature-dependent isotope fractionation after Tremaine et al. (2011).

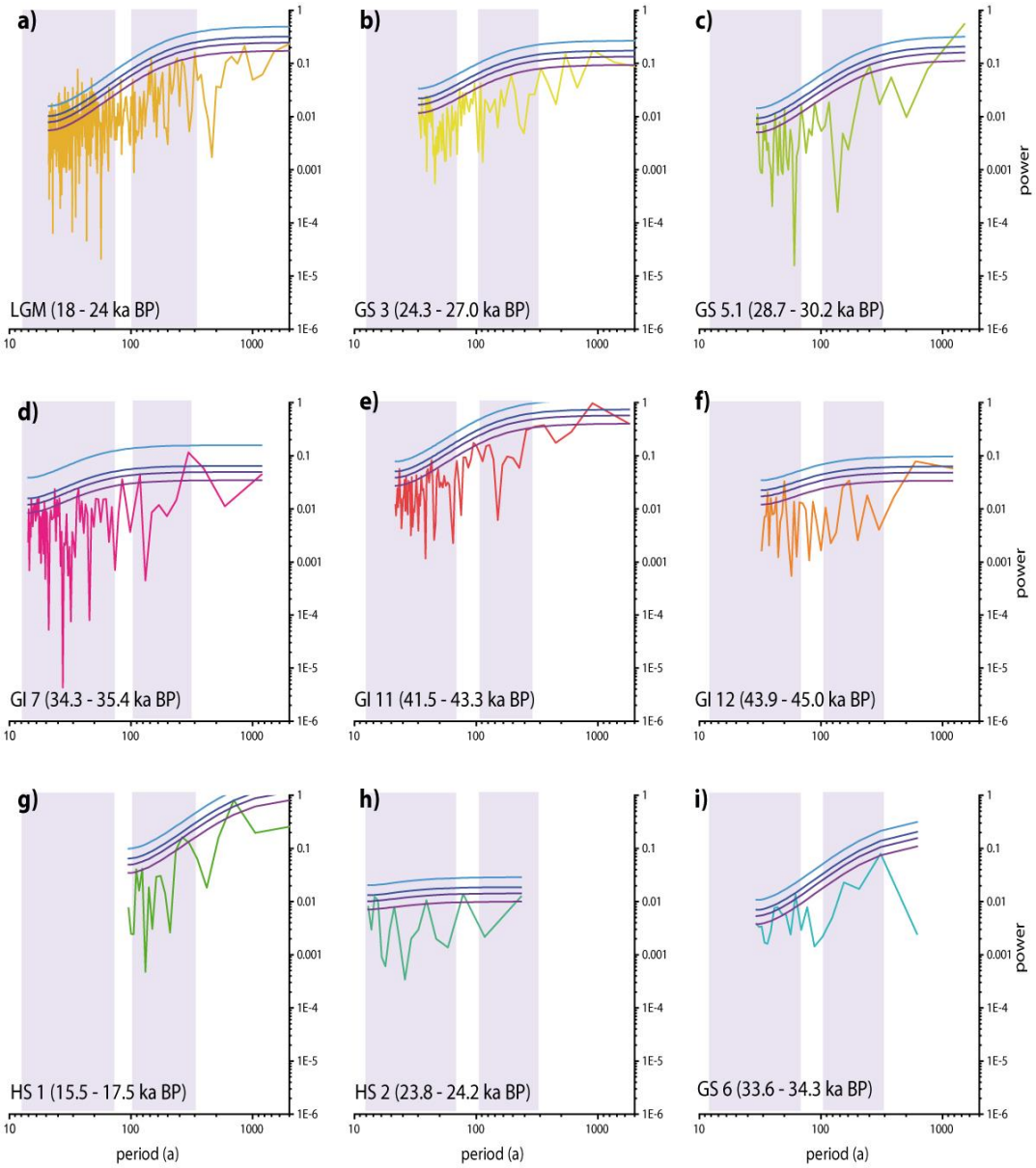

120 **Figure S5. Spectral power for different intervals of the PR-LA-1 $\delta^{13}C$ record calculated with REDFIT (Schulz & Mudelsee, 2002). Coloured lines indicate the calculated AR(1) false-alarm levels of 80% (purple), 90% (violet), 95% (dark blue) and 99% (light blue). Purple rectangles indicate the multi-decadal and centennial period bands. For all shown spectra, the AR(1) passed the REDFIT runs test which checks the equality of theoretical AR(1) and data spectrum.**

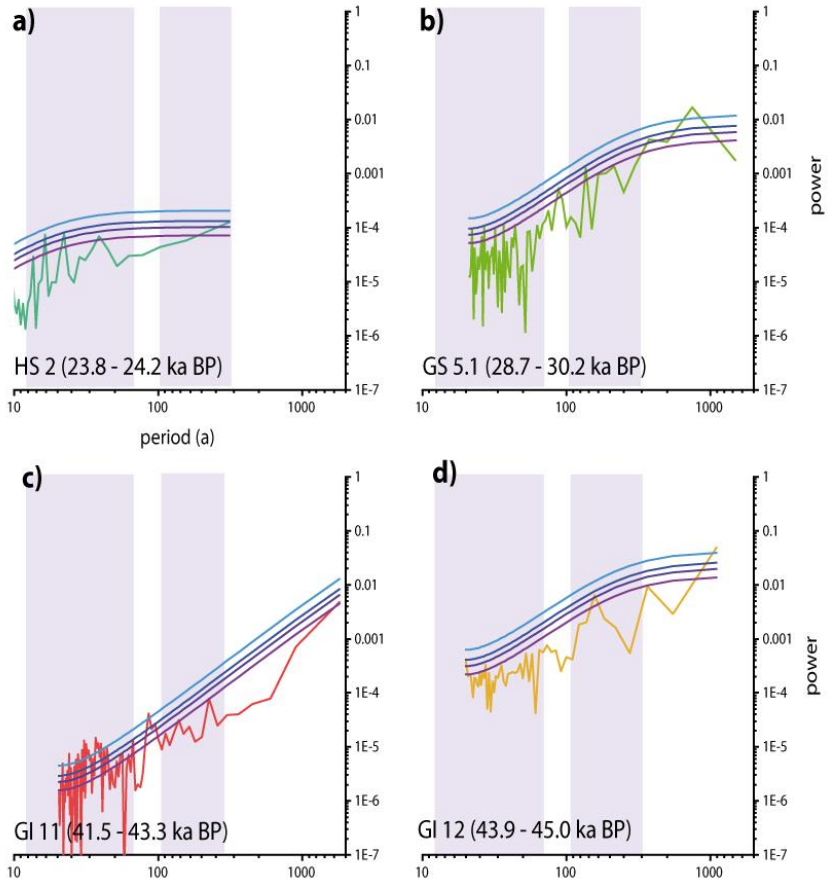

Figure S6. Spectral power for different intervals of the PR-LA-1 Mg/Ca record calculated with REDFIT (Schulz & Mudelsee, 2002). Coloured lines indicate the calculated AR(1) false-alarm levels of 80% (purple), 90% (violet), 95% (dark blue) and 99% (light blue). Purple rectangles indicate the multi-decadal and centennial period bands. For all shown spectra, the AR(1) passed the REDFIT runs test which checks the equality of theoretical AR(1) and data spectrum. For Mg/Ca, an appropriate AR(1) model could be only fitted for HS2, GS5.1 and GI 11 and 12.

References

Arienzo, M. M., Swart, P. K., Pourmand, A., Broad, K., Clement, A. C., Murphy, L. N., et al. (2015). Bahamian speleothem reveals temperature decrease associated with Heinrich stadials. *Earth and Planetary Science Letters, 430*, 377-386. doi:10.1016/j.epsl.2015.08.035

Cheng, H., Edwards, R. L., Hoff, J., Gallup, C. D., Richards, D. A., & Asmerom, Y. (2000). The half-lives of uranium-234 and thorium-230. *Chemical Geology, 169*(1-2), 17-33. doi:10.1016/s0009-2541(99)00157-6

Deininger, M., & Scholz, D. (2019). ISOLUTION 1.0: an ISOtope evoLUTION model describing the stable oxygen (δ 18 O) and carbon (δ 13 C) isotope values of speleothems. *International Journal of Speleology, 48*(1), 3.

Lea, D. W., Pak, D. K., Peterson, L. C., & Hughen, K. A. (2003). Synchroneity of tropical and high-latitude Atlantic temperatures over the last glacial termination. *Science, 301*(5638), 1361-1364. doi:10.1126/science.1088470

Miller, T. E. (2010). Stream Pirates of the Caribbean: Tanamá and Camuy Rivers in the Northern Karst of Puerto Rico. *Espeleorevista Puerto Rico, 2*, 8-13.

Schulz, M., & Mudelsee, M. (2002). REDFIT: estimating red-noise spectra directly from unevenly spaced paleoclimatic time series. *Computers & Geosciences, 28*(3), 421-426.

Stoll, H. M., Müller, W., & Prieto, M. (2012). I-STAL, a model for interpretation of Mg/Ca, Sr/Ca and Ba/Ca variations in speleothems and its forward and inverse application on seasonal to millennial scales. *Geochemistry, Geophysics, Geosystems, 13*(9). doi:10.1029/2012gc004183

Tremaine, D. M., Froelich, P. N., & Wang, Y. (2011). Speleothem calcite farmed in situ: modern calibration of δ18O and δ13C paleoclimate proxies in a continuously-monitored natural cave system. *Geochimica et Cosmochimica Acta, 75*(17), 4929-4950.

Lab. No.	Sample	DFT [mm]	^{238}U [µg/g]	±	^{232}Th [ng/g]	±	$(^{234}U/^{238}U)$	±	$(^{230}Th/^{238}U)$	±	$(^{234}U/^{238}U)_{ini}$	±	Age_{uncorr} [ka]	±	Age_{corr} [ka]	±
SW111	L1A-0.5	0.5	0.2947	0.0035	0.4468	0.0049	1.107	0.012	0.1468	0.0031	1.111	0.012	16.45	0.28	15.48	0.39
SW1	L1A-1.5	1.5	0.2811	0.0017	0.1056	0.0015	1.1018	0.0018	0.1573	0.0013	1.1066	0.0019	17.00	0.14	16.76	0.15
SW41	L1A-2.5	2.5	0.1007	0.0006	0.0089	0.0002	1.0992	0.0044	0.1632	0.0015	1.1042	0.0046	17.50	0.19	17.48	0.19
SW9	L1A-5.3	5.3	0.3165	0.0021	0.0000	0.0000	1.0923	0.0025	0.1654	0.0014	1.0970	0.0026	17.86	0.16	17.86	0.16
SW2	L1A-6.5	6.5	0.3006	0.0016	0.0000	0.0000	1.0895	0.0015	0.1754	0.0013	1.0945	0.0015	19.10	0.15	19.10	0.15
SW17	L1A-9.5	9.5	0.3290	0.0019	0.0278	0.0004	1.0913	0.0016	0.1792	0.0010	1.0965	0.0017	19.57	0.12	19.52	0.13
SW10	L1A-10.8	10.8	0.2743	0.0019	0.4843	0.0060	1.0977	0.0043	0.1811	0.0033	1.1024	0.0045	20.75	0.19	19.61	0.41
SW42	L1A-11.8	11.8	0.0927	0.0006	0.0371	0.0005	1.0934	0.0046	0.1869	0.0020	1.0989	0.0048	20.46	0.26	20.39	0.25
SW11	L1A-16.1	16.1	0.2954	0.0022	0.0496	0.0024	1.0848	0.0047	0.1881	0.0017	1.0899	0.0049	20.82	0.23	20.71	0.24
SW25	L1A-17.5	17.5	0.2589	0.0015	0.0834	0.0011	1.0789	0.0024	0.1892	0.0016	1.0836	0.0024	21.19	0.19	20.98	0.20
SW3	L1A-19.5	19.5	0.3896	0.0023	0.7091	0.0075	1.0781	0.0015	0.1937	0.0032	1.0824	0.0016	22.73	0.13	21.54	0.41
SW33	L1A-20.3	20.3	0.2981	0.0018	0.1864	0.0028	1.0794	0.0017	0.1919	0.0020	1.0841	0.0018	21.70	0.22	21.30	0.26
SW43	L1A-21.3	21.3	0.1332	0.0008	0.0198	0.0003	1.0807	0.0033	0.1919	0.0016	1.0856	0.0035	21.31	0.21	21.27	0.21
SW18	L1A-23.2	23.2	0.3002	0.0016	1.721	0.017	1.0809	0.0017	0.2000	0.0099	1.0839	0.0018	26.06	0.16	22.3	1.3
SW26	L1A-25.2	25.2	0.3036	0.0018	2.027	0.020	1.0805	0.0025	0.2007	0.0116	1.0832	0.0027	26.79	0.17	22.3	1.5
SW4	L1A-26.5	26.5	0.3026	0.0018	0.1794	0.0027	1.0772	0.0014	0.1989	0.0021	1.0819	0.0015	22.59	0.24	22.20	0.27
SW12	L1A-31.7	31.7	0.3306	0.0028	0.0208	0.0022	1.0819	0.0063	0.2031	0.0018	1.0872	0.0068	22.66	0.27	22.61	0.27
SW19	L1A-32.5	32.5	0.3075	0.0018	0.0451	0.0006	1.0808	0.0016	0.2062	0.0016	1.0861	0.0017	23.12	0.21	23.03	0.21
SW5	L1A-35	35	0.3491	0.0022	n.d.	n.d.	1.0847	0.0017	0.2100	0.0014	1.0905	0.0018	23.39	0.18	23.39	0.18
SW6	L1A-41	41	0.3205	0.0020	n.d.	n.d.	1.0883	0.0018	0.2136	0.0012	1.0944	0.0019	23.76	0.16	23.76	0.16
SW13	L1A-47.8	47.8	0.2838	0.0018	n.d.	n.d.	1.0832	0.0023	0.2149	0.0020	1.0891	0.0025	24.05	0.27	24.05	0.27
SW14	L1A-49.3	49.3	0.2536	0.0017	n.d.	n.d.	1.0801	0.0035	0.2153	0.0019	1.0857	0.0037	24.17	0.26	24.17	0.26
SW20	L1A-50.8	50.8	0.2574	0.0015	0.1518	0.0020	1.0789	0.0017	0.2182	0.0020	1.0844	0.0018	24.96	0.22	24.58	0.25
SW15	L1A-54.5	54.5	0.2585	0.0017	0.1933	0.0028	1.0759	0.0032	0.2188	0.0018	1.0812	0.0034	25.21	0.19	24.72	0.25
SW29	L1B-0.00	55	0.2923	0.0032	0.02302	0.00062	1.073	0.010	0.2207	0.0028	1.078	0.010	25.10	0.45	25.05	0.45
SW44	L1B-4.0	59	0.3924	0.0024	0.00986	0.00018	1.0654	0.0042	0.2235	0.0019	1.0703	0.0044	25.63	0.27	25.61	0.27
SW49	L1B-5.5	60.5	0.2708	0.0023	0.0550	0.0014	1.0623	0.0066	0.2279	0.0039	1.0671	0.0073	26.41	0.55	26.27	0.53
SW34	L1B-9.3	64.3	0.3374	0.0020	0.01604	0.00053	1.0614	0.0020	0.2303	0.0020	1.0662	0.0021	26.64	0.27	26.61	0.27
SW50	L1B-10.8	65.8	0.3278	0.0026	0.03056	0.00066	1.0661	0.0061	0.2398	0.0033	1.0714	0.0067	27.77	0.46	27.71	0.48
SW145	L1B-13.2	68.2	0.3925	0.0023	0.0721	0.0012	1.0628	0.0018	0.2395	0.0019	1.0678	0.0019	27.89	0.25	27.77	0.26
SW27	L1B-17.7	72.7	0.4043	0.0024	0.02920	0.00072	1.0646	0.0025	0.2383	0.0026	1.0698	0.0027	27.61	0.35	27.56	0.35
SW51	L1B-19.7	74.7	0.3428	0.0038	0.02240	0.00069	1.071	0.010	0.2435	0.0036	1.077	0.011	28.09	0.57	28.04	0.57

SW45	L1B-24.0	79	0.1120	0.0007	0.03674	0.00050	1.0977	0.0039	0.2566	0.0021	1.1059	0.0041	28.99	0.29	28.92	0.29
SW28	L1B-25.3	80.3	0.2699	0.0017	0.05160	0.00077	1.0977	0.0027	0.2593	0.0021	1.1060	0.0029	29.39	0.28	29.27	0.29
SW105	L1C-1.5	82	0.4442	0.0030	n.d.	n.d.	1.0987	0.0045	0.2582	0.0021	1.1071	0.0048	29.09	0.31	29.09	0.31
SW35	L1C-2.7	83.2	0.4708	0.0027	0.00377	0.00046	1.0995	0.0018	0.2591	0.0020	1.1081	0.0020	29.19	0.27	29.18	0.26
SW106	L1C-6.2	86.7	0.3363	0.0032	n.d.	n.d.	1.1000	0.0084	0.2616	0.0026	1.1087	0.0089	29.49	0.43	29.49	0.43
SW146	L1C-8.9	89.4	0.3752	0.0021	0.05437	0.00072	1.1007	0.0016	0.2625	0.0019	1.1094	0.0018	29.68	0.25	29.59	0.25
SW46	L1C-10.6	91.1	0.0941	0.0006	0.00556	0.00014	1.1014	0.0050	0.2637	0.0027	1.1103	0.0053	29.72	0.38	29.71	0.37
SW52	L1C-11.7	92.2	0.3532	0.0037	0.00097	0.00029	1.1019	0.0099	0.2640	0.0032	1.111	0.011	29.74	0.52	29.74	0.53
SW147	L1C-14.2	94.7	0.3467	0.0020	0.03649	0.00056	1.0973	0.0017	0.2636	0.0021	1.1058	0.0018	29.91	0.28	29.84	0.28
SW107	L1C-16.3	96.8	0.3073	0.0030	0.0014	0.0011	1.0930	0.0088	0.2682	0.0029	1.1014	0.0094	30.58	0.48	30.57	0.49
SW30	L1C-19.9	100.4	0.3244	0.0022	0.00703	0.00030	1.0915	0.0040	0.2657	0.0025	1.0997	0.0043	30.31	0.35	30.30	0.35
SW47	L1C-22.7	103.2	0.2007	0.0013	0.01040	0.00017	1.0860	0.0032	0.2750	0.0020	1.0941	0.0035	31.74	0.29	31.72	0.29
SW108	L1C-24.3	104.8	0.3114	0.0037	0.0126	0.0014	1.085	0.011	0.2759	0.0034	1.093	0.012	31.90	0.59	31.87	0.60
SW 36	L1C-26.1	106.6	0.3411	0.0020	n.d.	n.d.	1.0706	0.0018	0.2819	0.0026	1.0776	0.0020	33.21	0.36	33.21	0.36
SW109	L1C-28.3	108.8	0.3370	0.0022	n.d.	n.d.	1.0687	0.0040	0.2839	0.0024	1.0756	0.0044	33.55	0.36	33.55	0.36
SW148*	L1C-33.4	113.9	0.3596	0.0020	0.07142	0.00086	1.0510	0.0017	0.2916	0.0020	1.0563	0.0018	35.46	0.28	35.33	0.29
SW110*	L1C-35.5	116	0.3140	0.0036	0.3373	0.0039	1.0494	0.0108	0.2889	0.0039	1.054	0.012	35.74	0.68	35.02	0.73
SW149*	L1C-37.0	117.5	0.3483	0.0020	0.0784	0.0009	1.0505	0.0020	0.2956	0.0025	1.0558	0.0021	36.08	0.37	35.93	0.37
SW31	L1C-38.5	119	0.3637	0.0025	0.01813	0.00040	1.0541	0.0044	0.2833	0.0033	1.0596	0.0048	34.07	0.50	34.03	0.51
SW113	L1D-0.0	120.6	0.3443	0.0019	n.d.	n.d.	1.0469	0.0015	0.2758	0.0037	1.0515	0.0016	33.27	0.53	33.27	0.53
SW129*	L1D-3.2	123.8	0.2682	0.0016	0.2061	0.0025	1.0719	0.0017	0.3590	0.0031	1.0811	0.0018	44.75	0.42	44.25	0.48
SW114	L1D-7.4	128	0.3484	0.0020	0.00160	0.00093	1.0448	0.0016	0.2850	0.0040	1.0494	0.0018	34.66	0.56	34.66	0.57
SW130*	L1D-10.2	130.8	0.1967	0.0011	1.455	0.015	1.0808	0.0022	0.3776	0.0136	1.0891	0.0025	51.50	0.41	46.59	2.32
SW115	L1D-13.0	133.6	0.3398	0.0019	0.0301	0.0011	1.0529	0.0017	0.2873	0.0034	1.0583	0.0018	34.71	0.47	34.65	0.48
SW131*	L1D-17.1	137.7	0.2364	0.0014	1.029	0.010	1.0711	0.0020	0.3757	0.0080	1.0796	0.0023	49.74	0.34	46.9	1.4
SW132*	L1D-18.3	138.9	0.2265	0.0013	0.05063	0.00088	1.0719	0.0017	0.3492	0.0027	1.0811	0.0019	42.93	0.39	42.78	0.40
SW116	L1D-23.7	144.3	0.3783	0.0022	n.d.	n.d.	1.0770	0.0018	0.3003	0.0028	1.0852	0.0020	35.50	0.40	35.50	0.40
SW125	L1E-1.2	146.2	0.2887	0.0016	0.01636	0.00052	1.0953	0.0016	0.3485	0.0022	1.1071	0.0017	41.55	0.33	41.51	0.34
SW133	L1E-5.9	150.9	0.2025	0.0012	0.00910	0.00042	1.0952	0.0016	0.3468	0.0023	1.1069	0.0018	41.31	0.32	41.28	0.34
SW134	L1E-10.9	155.9	0.2961	0.0017	0.03165	0.00060	1.0778	0.0018	0.3541	0.0030	1.0879	0.0021	43.28	0.46	43.21	0.45
SW126	L1E-11.9	156.9	0.3274	0.0019	0.03503	0.00066	1.0778	0.0018	0.3543	0.0030	1.0879	0.0021	43.30	0.44	43.23	0.46
SW127	L1E-14.0	159	0.3358	0.0019	0.4433	0.0060	1.0796	0.0017	0.3528	0.0036	1.0894	0.0019	43.77	0.42	42.91	0.57
SW124	L1E-19.2	164.2	0.3346	0.0019	0.0776	0.0013	1.0719	0.0017	0.3504	0.0026	1.0811	0.0019	43.11	0.40	42.96	0.40

SW135	L1Eb-0.7	166.8	0.3227	0.0018	0.4264	0.0058	1.0796	0.0017	0.3528	0.0036	1.0894	0.0018	43.78	0.42	42.92	0.57
SW117*	L1Eb-2.2	168.3	0.3328	0.0019	0.0479	0.0015	1.0709	0.0016	0.3334	0.0047	1.0794	0.0017	40.58	0.68	40.49	0.69
SW121	L1Eb-4.1	170.2	0.2882	0.0016	0.2222	0.0026	1.0719	0.0017	0.3593	0.0031	1.0812	0.0019	44.80	0.44	44.29	0.49
SW150	L1Eb-8.2	174.3	0.2950	0.0023	0.9855	0.0099	1.0679	0.0060	0.3502	0.0067	1.0756	0.0069	45.35	0.58	43.1	1.1
SW122	L1Eb-10.1	176.2	0.2493	0.0014	1.845	0.019	1.0808	0.0022	0.378	0.014	1.0891	0.0026	51.58	0.41	46.7	2.4
SW123	L1Eb11.1	177.2	0.2385	0.0014	1.038	0.011	1.0711	0.0020	0.3757	0.0080	1.0796	0.0022	49.74	0.34	46.9	1.3
SW151*	L1Eb-12.5	178.6	0.2475	0.0015	0.1712	0.0023	1.0696	0.0023	0.3861	0.0039	1.0796	0.0026	49.03	0.60	48.57	0.63
SW118	L1Eb-15.2	181.3	0.2816	0.0016	0.1937	0.0027	1.0700	0.0016	0.3669	0.0043	1.0793	0.0018	46.01	0.64	45.56	0.66
SW119	L1Eb-20.7	186.8	0.3081	0.0017	n.d.	n.d.	1.0724	0.0017	0.3694	0.0042	1.0825	0.0019	45.81	0.64	45.81	0.64

Table S2. Activity ratios and calculated ages of stalagmite PR-LA-1.

Activity ratios were corrected for initial Th assuming an detrital weight ratio $^{232}Th/^{238}U = 0.154 \pm 0.038$ (corresponding to an activity ratio of the detritus in secular equilibrium of $(^{230}Th/^{232}Th) = 19.79 \pm 4.93$, and secular equilibrium of the detritus.

Ages are calculated using the decay constants by Cheng et al. (2000)).

Uncertainties are given as 2σ- range, and do not include half-life uncertainties.

Ages marked with a * are not used to calculate the age model